Small-molecule inhibitors of the PDZ domain of Dishevelled proteins interrupt Wnt signalling

Nestor Kamdem [1,2], Yvette Roske [3], Dmytro Kovalskyy [4,6] Maxim O. Platonov [4,6], Oleksii Balinskyi [4,6], Annika Kreuchwig [1,2], Jörn Saupe [1,2], Liang Fang [2,3], Anne Diehl [1], Peter Schmieder [1], Gerd Krause [1], Jörg Rademann [1,5], Udo Heinemann [2,3], Walter Birchmeier [3] and Hartmut Oschkinat [1,2].

[1] Leibniz-Forschungsinstitut für Molekulare Pharmakologie, Robert-Rössle-Straße 10, 13125 Berlin, Germany
[2] Institut für Chemie und Biochemie, Freie Universität Berlin, Takustraße 3, 14195 Berlin, Germany
[3] Max-Delbrück-Center for Molecular Medicine, Robert-Rössle-Straße 10, 13125 Berlin, Germany
[4] Enamine Ltd., Chervonotkatska Street 78, Kyiv 02094, Ukraine
[5] Institut für Pharmazie, Freie Universität Berlin, Königin-Luise-Straße 2 + 4, 14195 Berlin, Germany
[6] Taras Shevchenko National University, 62 Volodymyrska, Kyiv 01033, Ukraine

Correspondence to: Hartmut Oschkinat (oschkinat@fmp-berlin.de)

Abstract

Dishevelled (Dvl) proteins are important regulators of the Wnt signalling pathway, interacting through their PDZ domains with the Wnt receptor Frizzled. Blocking the Dvl PDZ/Frizzled interaction represents a potential approach for cancer treatment, which stimulated the identification of small molecule inhibitors, among them the anti-inflammatory drug Sulindac and Ky-02327. Aiming to develop tighter binding compounds without side effects, we investigated structure-activity relationships of sulfonamides. X-ray crystallography showed high complementarity of anthranilic acid derivatives in the GLGF loop cavity and space for ligand growth towards the PDZ surface**.** Our best binding compound inhibits Wnt signalling in a dose-dependent manner as demonstrated by TOP-GFP assays (IC_{50} ~50 μM), and Western blotting of β-catenin levels. Real-time PCR showed reduction in the expression of Wnt-specific genes. Our compound interacted with Dvl-1 PDZ (K_D=2.4 μM) stronger than Ky-02327 and may be developed into a lead compound interfering with the Wnt pathway.

KEYWORDS: Drug Design, NMR, PDZ, Frizzled, Wnt signalling

INTRODUCTION

Dishevelled (Dvl) proteins comprise 500 to 600 amino acids and contain three conserved domains: an N-terminal DIX (**Di**shevelled/A**x**in) domain (Schwarz-Romond 2007, Madrzak 2015), a central PDZ (**P**SD95/**D**lg1/**Z**O-1) domain (Doyle 1996, Ponting 1997), and a C-terminal DEP (**D**ishevelled/**E**gl-10/**P**leckstrin) domain (Wong 2000, Wallingford 2005). Dvl transduces Wnt signals from the membrane receptor Frizzled to downstream components *via* the interaction between Dvl PDZ and Frizzled (Wong 2003), thus it has been proposed as drug target (Klaus 2008, Holland 2013, Polakis 2012). Several studies identified internal peptides of the type (KTXXXW) as well as C-terminal peptides of the type (ΩΦGWF) in which Ω is any aromatic amino acid (F, W or Y) as Dvl PDZ targets (Lee 2009, Zhang 2009). Three Dvl homologues, Dvl-1, Dvl-2 and Dvl-3, have been identified in humans. Sequence identity is 88% between Dvl-3 PDZ and Dvl-1 PDZ and 96% between Dvl-3 PDZ and Dvl-2 PDZ (Supporting Information Figure S1). Dvl proteins are found to be upregulated in breast, colon, prostate, mesothelium, and lung cancers (Weeraratna 2002, Uematsu 2003, Bui 1997, Mizutani 2005).

PDZ domains appear in 440 copies spread over more than 260 proteins of the human proteome (Ponting 1997). They maintain relatively specific protein-protein interactions and are involved, for example, in signalling pathways, membrane trafficking and in the formation of cell-cell junctions (Zhang 2003, Fanning 1996, Kurakin 2007). Hence, they are potentially attractive drug targets (Rimbault 2019, Christensen 2020). PDZ domains consist of about 90 amino acids which fold into two α-helices and six β-strands exposing a distinct peptide-binding groove (Doyle 1996, Lee 2017). The conserved carboxylate-binding loop (GLGF loop, FLGI in Dvl-2 and -3, Figure 1) is essential for the formation of a hydrogen bonding network between the PDZ domain and PDZ-binding, C-terminal peptide motifs, in most cases coordinating the C-terminal carboxylate group of the interaction partner. In the respective complexes, the C-terminal residue of the ligand is referred to as P_0; subsequent residues towards the N-terminus are termed P_{-1}, P_{-2}, and P_{-3} etc. Previous studies have revealed that P_0 and P_{-2} are most critical for PDZ-ligand recognition (Songyang 1997, Schultz 1998).

PDZ domains are divided into at least three main classes on the basis of their amino acid preferences at these two sites: class I PDZ domains recognize the motif S/T-X-Φ-COOH (Φ is a hydrophobic residue and X any amino acid). Class II PDZ domains recognize the motif Φ-X-Φ-COOH, whereas class III

PDZ domains recognize the motif X-X-COOH. However, some PDZ domains do not fall into any of these specific classes (Pawson 2007, Sheng 2001, Zhang 2003). The Dvl PDZ domains, for example, recognize the internal sequence (KTXXXW) within the frizzled peptide 525(GKTLQSWRRFYH)536 (K_D ~ 10 μM) (Wong 2003, Chandanamali 2009).

Due to their occurrence in important proteins, PDZ domains received early attention as drug targets, nicely summarized in Christensen 2019. There are several examples of Dvl PDZ inhibitors of peptide or peptidomimetic nature (eg. Hammond 2006, Haugaard-Kedstrom 2021), including peptide conjugates (eg. Qin 2021, Hegedus 2021), and on an organic, small-molecule basis. The latter approach is considered most beneficial in long term medical treatments of conditions like cancer or neurological disorders. NSC668036 (Shan 2005, Wang 2015) is a peptide-mimic compound which interferes with Wnt signalling at the Dvl level. Based on a computational pharmacophore model of NCS668036, additional compounds were later reported (Shan 2012). Known as first non-peptide inhibitor, the 1H-indole-5-carboxylic acid derivative FJ9 (Fujii 2007) showed therapeutic potential. Further examples including Sulindac (Lee 2009), 2-((3-(2-Phenylacetyl)amino)benzoyl)amino)benzoic acid (3289-8625, also called CalBioChem(CBC)-322338) (Grandy 2009, Hori 2018), N-benzoyl-2-amino-benzoic acid analogs (Hori 2018), phenoxyacetic acid analogs (Choi 2016), and Ethyl 5-hydroxy-1-(2-oxo-2-((2-(piperidin-1-yl)ethyl)amino)ethyl)-1H-indole-2-carboxylate (KY-02327) (Kim 2016) have been reported, with the latter showing the highest *in-vitro* affinity (8.3 μM) of all. Despite the existence of the abovementioned inhibitors of Dvl PDZ, the development of tighter-binding, non-peptidic small-compound modulators of the respective functions, binding with nanomolar affinity, is necessary and remains challenging. On this path, we explore optimal fits for the primary binding pocket by cycles of chemical synthesis and X-ray crystallography and further avenues for systematically growing ligands along the Dvl PDZ surface to provide SAR for the development of inhibitors in the low or medium nanomolar range. Nuclear magnetic resonance (NMR) spectroscopy was used to detect primary hits and for follow-up secondary screening. The ability of NMR to detect weak intermolecular interactions (μM < K_D < mM) make it an ideal screening tool for identifying and characterizing weakly binding fragments, to be optimized subsequently by chemical modification in order to improve binding (Zartler 2006, Shuker 1996, Zartler 2003). Besides NMR, the determination of X-ray crystal structures of selected

complexes was fundamental for further design of new compound structures with improved binding. In the first round of screening, a library constructed after computational docking of candidates into the peptide binding site of the Dvl PDZ domains were investigated, followed by secondary screening utilizing a library of 120 compounds containing rhodanine or pyrrolidine-2,5-dione moieties.

RESULTS AND DISCUSSION

PDZ targeted library design

The PDZ targeted library was designed to cover all PDZ domains with available structure. For this, all X-ray and NMR derived PDZ structures were retrieved from the PDB, clustered, and 6 selected centroids were subjected to the virtual screening routine. The area considered is shown in Figure 1A, with the blue sphere indicating the geometrical centre. The clustering of the PDZ domains was performed according to the shapes of their binding sites, rather than backbone conformation. This approach accounts for the importance of surface complementarity of protein-small molecule interactions and the critical contribution of van der Waals interactions to the binding free energy. On another hand, PDZ domains have evolved to recognize a carboxyl group that is mostly derived from the C-terminus of natively binding proteins. Finally, the fact that PDZ can recognize internal motifs (Hillier 1999), including KTXXXW of Frizzled-7 recognised by Dvl PDZ (Wong 2003, Chandanamali 2009), raises the question of what are key binding contributions with PDZ domains: negative charge, hydrogen bonding or shape complementarity (Harris 2003). For this reason, tangible compounds were preselected to have extensive hydrophobic contacts as well as chemical groups that mimic the carboxylic group.

Virtual screening was performed with QXP, and the generated complexes were sequentially filtered with a self-designed MultiFilter algorithm. From the resulting 1119 compounds a randomly selected set of 250 compounds was subjected to NMR validation.

NMR Screening and development of compounds

The results of virtual screening were checked experimentally by comparing 2D ^{1}H-^{15}N HSQC (Heteronuclear Single Quantum Correlation) spectra of Dvl-3 PDZ in the absence and presence of the compound to elucidate ligand-induced changes of chemical shifts. Chemical shift perturbation

differences (ΔCSP, representing the average of the three strongest shifting cross peaks according to equation 1) were evaluated in cases where the residues responding strongest are inside the area defined by Figure 1A. The responses were classified into: (i) inactive compounds (ΔCSP < 0.02); (ii) very weak interactions (0.02 ≤ ΔCSP ≤ 0.05); (iii) weak interactions (0.05 < ΔCSP ≤ 0.1); (iv) intermediate interactions (0.1 < ΔCSP ≤ 0.2); (v): strong interactions (0.2 < ΔCSP ≤ 0.5) and (vi) very strong interactions (ΔCSP > 0.5). In most cases, the signals of residues S263, V287 and R320 (Figure 1A) within the conserved binding site were most strongly perturbed (Supporting Information Figure S2). With the ΔCSP of 0.12 ppm, the isoleucine-derived compound **1** ((2,3-dihydrobenzo[b][1,4]dioxin-6-yl)sulfonyl)-L-isoleucine containing a sulfonamide moiety was detected initially as one of the best "hits" according to chemical shift changes. The sulfonamide is a well-known moiety in drug discovery (Mathvink 1999, Wu 1999, Sleight 1998 O'Brien 2000, Tellew 2003).

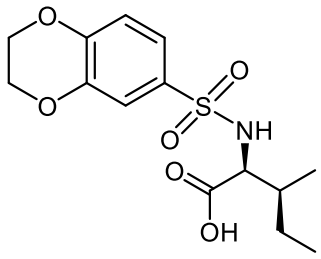

1

Upon NMR titration experiments for compound **1** (Supporting Information Figure S2) with Dvl-3 PDZ, the largest chemical shift perturbations were observed for S263 in strand βB and R320 in helix αB of Dvl-3 PDZ, confirming the conserved binding site.

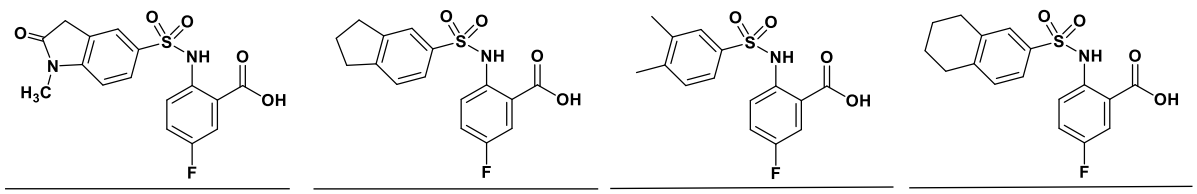

2 **3** **4** **5**

Scheme 1: Compounds **2**, **3**, **4**, **5**

By comparing the binding of several sulfonamide compounds in a secondary screening event and making use of our in-house library, four new compounds (**2**, **3**, **4, 5**) that induced chemical shift perturbations larger than 0.2 ppm were found (for binding constants see Table 1) and considered further as reasonably

strong binders. The similarity of the structures led us to define Scheme 2 as a scaffold for further refinements. Sulfonamides were considered more drug-like, and hence followed up at higher priority than other hits. We realised that our four new compounds had different moieties at R_2 in combination with a small R_1 (fluorine). A decrease of binding was observed with decreasing size of R_2.

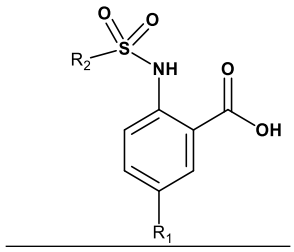

Scheme 2: Basic fragment for further synthesis

In order to assess the importance of the aryl group at R_2 for complex formation, it was replaced by a methyl group as substituent to yield compound **6**, which showed a drastic decrease of binding (Table 1). Compounds **3**, **4**, and **5** did not distinguish between the Dvl-3 PDZ and Dvl-1 PDZ. In order to obtain detailed insight into the binding mode of these compounds, crystal structures of Dvl-3 PDZ in complex with compounds **3**, **5** and **6** were determined (Figure 1). For compound **3** the crystal structure revealed two complexes within the crystallographic asymmetric unit (AU) at 1.43 Å resolution. Both show the anthranilic acid with the attached fluorine pointing into the hydrophobic binding pocket (Figure 1B and Supporting Information Figure S3A), while the carboxyl group forms a hydrogen-bond network with amide residues of the carboxylate binding loop, in particular strand βB (Figure 1B) and specifically with residues I262, G261 and L260. The two sulfonamide oxygen atoms form hydrogen bonds with R320 and H324 (weak) of helix αB for only one complex in the AU. The aromatic aryl group (tetrahydronaphtalene) attached to the sulfonamide is involved in hydrophobic interactions with F259 (Supporting Information Figure S3B). The 1.6-Å complex structure with compound **5** (4 molecules per AU) exhibits a comparable binding mode as found for compound **3** with a hydrogen-bond network involving the carboxyl group and the amides of I262, G261, L260, and of the sulfonamide to H324 (Figure 1C). No hydrogen bond was observed to R320 in all four molecules of the AU, but small variations of the aryl moiety relative to F259 (Supporting Information Figure S3C). The crystals of the complex with **6** show two molecules in the AU (Figure 1D). The sulfonamide is bound by H324 in both

complexes (Supporting Information Figure S3D). However, compound **6** bound only in the mM range as compared to **3** and **5**, which obviously results from the missing aromatic rings.

	ID	R_1	R_2	(K_D, µM) Dvl-3PDZ	(K_D, µM) Dvl-1 PDZ
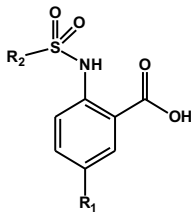	2	F	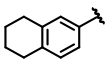	nd	237.6 ± 38.5^{NMR}
	3	F		80.6 ± 6.1^{NMR}	112.7 ± 25.9^{NMR}
	4	F		83.9 ± 7.8^{NMR}	114.4 ± 9.8^{NMR}
	5	F		140.6 ± 14.1^{NMR}	160.1 ± 14.6^{NMR}
	6	F	CH_3	$> 1000^{ITC}$	-
	7	Br	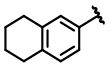	20.6 ± 2.4^{NMR}	18.2 ± 2.4^{NMR}
	8	CF_3	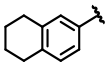	17.4 ± 0.5^{ITC}	24.5 ± 1.5^{ITC}
	9	Cl	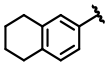	41.1 ± 3.1^{NMR}	45.6 ± 4.5^{NMR}
	10	CH_3	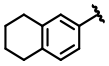	62.5 ± 4.7^{NMR}	60.5 ± 5.3^{NMR}
	11	Br	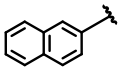	13.8^{ITC}	119.9^{ITC}
	12	Br		58.5^{ITC}	nd
	13	Br	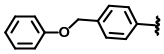	7.2^{ITC}	213.2^{ITC}
	14	Br		58.1 ± 2.1^{ITC}	nd
	15	CF_3		52.9 ± 1.7^{ITC}	nd
	16	CF_3	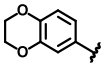	59.1 ± 1.5^{ITC}	nd
	17	CF_3		49.5^{ITC}	nd
	18	CH_3	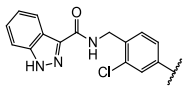	9.4 ± 0.6^{ITC}	2.4 ± 0.2^{ITC}
	19	CH_3	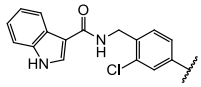	21.8 ± 1.7^{ITC}	8.0 ± 0.5^{ITC}
	20	CH_3	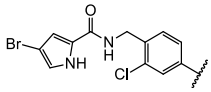	9.8 ± 0.3^{ITC}	4.7 ± 0.3^{ITC}
	21	CH_3	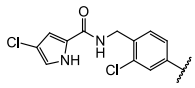	12.5 ± 0.5^{ITC}	4.7 ± 0.2^{ITC}

Table 1. Binding constants K_D (µM) of Dvl-3 PDZ and Dvl-1 PDZ for compounds 3 – 21 derived by ITC or NMR if not specified. The K_D values determined by NMR are reported as means ± standard deviations of measurements evalutating shifts of cross peaks of at least six residues influenced upon binding of the ligand. The K_D values ($1/K_A$) determined by ITC were obtained as fits to a one-site binding model (n in the range of 0.95-1.2) with K_D errors obtained by $\Delta K_A/K_A^2$.

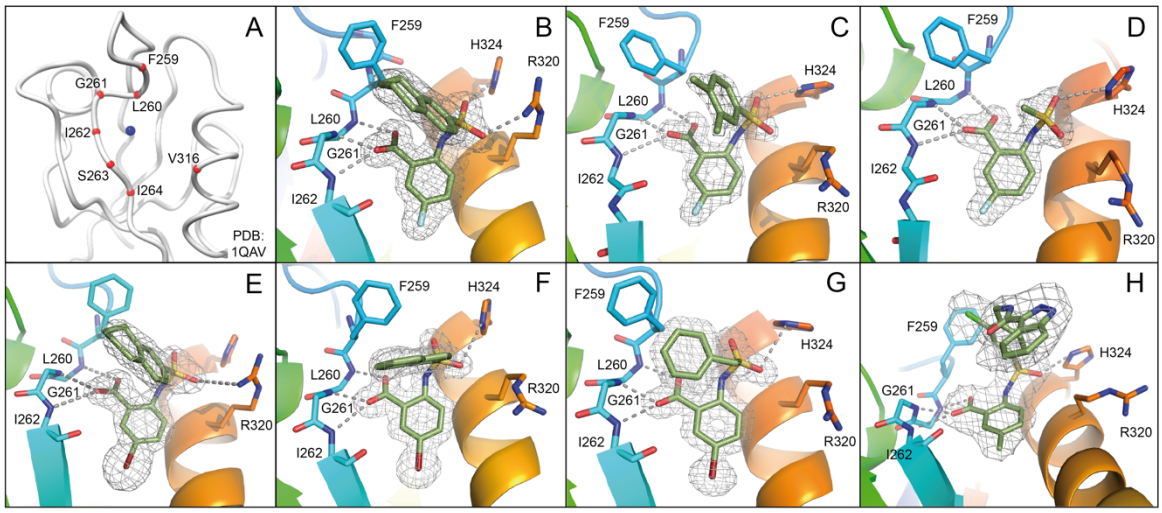

Figure 1: **A** Definition of PDZ binding site. The center of the binding site (blue sphere) is defined as the geometric center of Cα atoms (red spheres) of 7 residues (typed in red) defined by multiple sequence alignment. **B-H** Magnified views into crystal structures of various compounds bound to the Dvl-3 PDZ domain. The 2Fo-Fc electron density around the compounds is shown at 1σ contour level, and the dotted lines indicate formed hydrogen bonds. In the bound compounds covalent bonds to carbon atoms are shown as green sticks. Important residues involved in compound binding are labelled and displayed in atom colours (carbons blue or dark yellow). **B-D** show compound **3**, **5** and **6** respectively. All compounds in **B-D** contain fluorine (light blue) in para position to the amine. **E-G** represents the bound compounds **7**, **11** and **12**, respectively. All have bromine (dark red) in para position to the amine. **H** shows compound **18** within the binding site. The accession codes of the structures B-H are 6ZBQ, 6ZBZ, 6ZC3, 6ZC4, 6ZC6, 6ZC7 and 6ZC8, respectively.

To further explore the importance of the fluorine site inside the hydrophobic pocket, substitutions by bromine, chlorine, methyl and trifluoromethyl were chosen. In fact, the methyl group has a similar vdW radius as the CF_3 group. Iodine was not considered a good candidate since it increases molecular weight substantially and the compounds may be chemically less stable, in particular in biological assays. Taking into account that compound **6** did not bind because of the missing aromatic ring at the R_2 position, our overall strategy was to increase the aromatic ring at R_2 while finding a good fit for R_1, keeping an eye on the molecular weight to enable further compound modifications that fulfil key properties as defined by Lipinski (Lipinski 2000, Lipinski 1997). Our preference to continue exploration at the R_1 position of the aromatic ring in Scheme 1 was inspired by the absence of hits with other substitutions in the secondary screening event and the initial X-ray structures that showed a hydrophobic pocket available for substituents in this position while other sites at the aromatic ring would include steric hindrance. Therefore, compounds **7-17** were obtained and were classified in three different groups to derive structure activity relationships (SAR). The compounds **7-10** in group 1 contain different R_1 (Br, CF_3, Cl, CH_3) but the same moiety (tetrahydronaphthalene) at R_2. As expected, binding could be further improved by displacement of the fluorine with elements exhibiting larger van der Waals (vdW) radii.

Indeed, the K_D decreased stepwise and the best fit was observed for compound **8** containing a trifluoromethyl group (K_D = 17.4 μM for Dvl-3 PDZ and 24.5 μM for Dvl-1 PDZ). The different substituents at the R_1 position contribute to an increased binding affinity in the following order: F < Cl < Br < CF_3 (compound **3** < **9** < **7**< **8**, respectively). Compound **10** with a methyl group at the R_1 position showed only marginally improved binding, although the methyl group has a similar vdW radius as the CF_3 group of compound **8**. The difference in binding results most likely from their different hydrophobicity.

The 1.85-Å crystal structure of the Dvl-3 PDZ domain with compound **7** (K_D = 20.6 μM for Dvl-3 PDZ and 18.2 μM for Dvl-1 PDZ) showed an identical hydrogen-bond network involving the amide groups of residues I262, G261 and L260 of the carboxyl binding loop as seen for all other complex structures reported here (Figure 1E). Only one hydrogen bond between the sulfonamide and R320 was found in addition for one of the two Dvl-3 PDZ molecules per AU. H324 of Dvl-3 PDZ was not addressed by the sulfonamide as seen previously. The bromine at position R_1 points into the hydrophobic pocket, similar as the fluorine in the complex structure with compound **3**. The two complexes in the AU show significant variations in the positions of the tetrahydronaphtalene rings as well as for the side chain of F259 and R320 (Supporting Information Figure S3E).

Following the analysis of the complex involving compound **7**, the binding characteristics of the group-2 compounds (**11-14**) were investigated. They contain bromine as R_1 and different substituents at the R_2 position to assess the importance of π-π stacking interactions involving F259. K_D values of 7.2 μM for compound **13** and 13.8 μM for compound **11** were found with respect to the interaction with Dvl-3 PDZ. Crystal structures of Dvl-3 PDZ in complex with compound **11** (1.58 Å resolution, 1 molecule per AU) and **12** (1.48 Å, 2 molecules per AU) revealed very similar binding as observed in the crystal structures with compounds **3** and **7**. The aromatic rings at R_2 show hydrophobic interactions to F259, but not a classical π-π stacking as expected. Nevertheless, the tighter binding of compound **11** could be explained by the larger aromatic substituent at the R_2 position compared to compound **12**. Both complex structures show also non-specifically bound ligands in crystal contacts (Supporting Information Figure S3H, Supporting Information Tables S2 and S3). The additional ligand molecules in both complex structures can be explained as a crystallographic artefact, which is verified with ITC experiments that indicate 1:1

stoichiometries in both cases (Figure S5). With respect to the selectivity of the tested compounds we observed a 6 to 30-fold stronger binding of compounds **7**, **9**, **11** and **13** to Dvl-3 PDZ as compared to Dvl-1 PDZ. These differences are related to the different sequences at the end of αB. Most importantly, H324 is replaced by a serine residue in the Dvl-1 PDZ domain.

The group-3 compounds **(15-17)** contain a trifluoromethyl at position R_1 and were tested to investigate a cooperative role of this moiety with various substituents at position R_2. All compounds bind weaker to Dvl-1 and Dvl-3 than compound **8** which contains tetrahydronaphthalene at the R_1 position, revealing its important role in the interaction.

Further modifications towards higher affinity and reduced toxicity

Possible cytotoxic effects of compounds **3**, **7**, **8, 9**, and **10** were evaluated in cell viability assays using HEK293 cells (Supporting Information Figure S4). These compounds were selected due to different substituents at the R_1, including halogens. Cell viability was measured 24h after treatment with the individual compounds, and half maximal inhibitory concentrations (EC_{50}) were calculated for each compound. The compounds exhibited EC_{50} values in the range of 61-131 μM (Supporting Information Figure S4A). Compounds **3** and **10** that contained fluorine or methyl group substituents at R_2, respectively, were the least toxic, while compound **7**, containing bromine, was the most toxic. The results from crystallography, modelling studies and of the cell proliferation assays led us to further investigate compounds **18-21** that contain a methyl group at the R_1 position and different substituents as R_2. In this way, we aimed to develop both potent and less toxic, cell permeable inhibitors. All compounds showed strong interactions as indicated by chemical shift perturbation values between 0.30 to 0.34 ppm (Supporting Information Table S1). The binding constants were evaluated by ITC whereby compound **18** (K_D = 9.4 μM for Dvl-3 PDZ and 2.4 μM for Dvl-1 PDZ) appeared to be most potent. Compound **18** contains a pyrazole ring which is considered as an important biologically active heterocyclic moiety (Lv 2010). Compounds **20** (K_D = 9.8 μM for Dvl-3 PDZ and 4.7 μM for Dvl-1 PDZ) and **21** (K_D = 12.5 μM for Dvl-3 PDZ and 4.7 μM for Dvl-1 PDZ) contain pyrrole rings. Their binding constants almost have the same value despite the different substituents (bromine or chlorine) at the pyrrole rings. The binding of compounds **18**-**21** to both Dvl PDZ domains is mainly enthalpy-driven as

indicated in Table **2**, with a slightly stronger effect for Dvl-1 PDZ than for Dvl-3 PDZ. To our surprise, the crystal structure of Dvl-3 PDZ in complex with compound **18** shows the pyrazole substituent in the R_2 position orientated away from the binding pocket. Instead, a π-π stacking interaction with F259 was observed (Supporting Information Figure S3I). Cytotoxicity of **18**-**21** was determined *via* MTT assays (Mosmann 1983) that displayed viability up to concentrations above 150 μM (Supporting Information Figure S4B).

Compound	Dvl-3 PDZ				Dvl-1 PDZ			
	K_D (μM)	ΔH (kcal/ mol)	TΔS (kcal/ mol)	ΔG (kcal/ mol)	K_D (μM)	ΔH (kcal/ mol)	TΔS (kcal/ mol)	ΔG (kcal/ mol)
18	9.4 ± 0.6	-8.0	-1.2	-6.8	2.4 ± 0.2	-12.2	-4.7	-7.5
19	21.0 ± 1.7	-5.9	0.4	-5.5	8.0 ± 0.5	-7.3	-0.3	-7.0
20	9.8 ± 0.3	-10.4	-3.6	-6.8	4.7 ± 0.3	-9.4	-2.2	-7.2
21	12.5 ± 0.5	-5.9	0.7	-6.8	4.7 ± 0.2	-8.5	-1.5	-7.0
NPL-1011	79.7 ± 53.3							
Sulindac	8.3 ± 2.5							
CBC-322338/ 3289-8625	> 400 μM							
NSC668036	> 400 μM							
Ky-02327					8.3 ± 0.8[16g]			

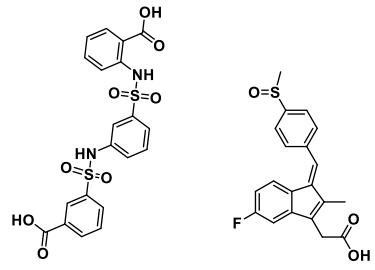
NPL-1011

Sulindac

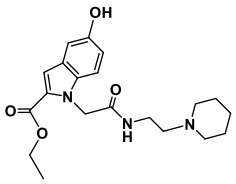
Ky-02327

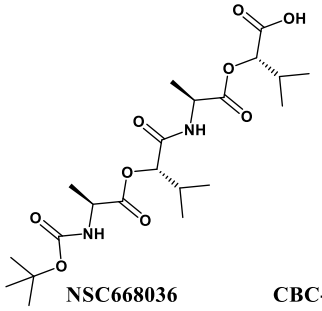
NSC668036

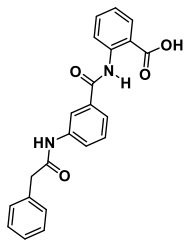
CBC-322338 / 3289-8625

Table 2: Isothermal titration calorimetric data for the reaction between Dvl-3 PDZ, Dvl-1 PDZ and our compounds **18**, **19**, **20** and **21** respectively. Compounds NPL-1011 (Hori 2018), and Sulindac (Lee 2009), CBC-322338/3289-8625 (Grandy 2009, Hori 2018), and NSC668036 (Shan 2005), for more thermodynamic parameters see Supporting Information Figure S7. For Ky-02327 the value from literature is included.

Comparison to reported Dvl PDZ-binding molecules

Our compounds bind to Dvl-3 with a K_D better than 10 μM, and slightly tighter to Dvl-1, see Table 2, with **18** showing a K_D of 2.4 μM and chemical shift changes indicating binding to the canonical binding site (Figure 1A). For comparison, four compounds of those shown in Supporting Information Figure S6 were assayed by ITC (Supporting Information Figure S7) regarding their affinity to Dvl-3 PDZ. Ky-02327 was already determined to bind with a K_D of 8.3 ± 0.8 μM (Kim 2016) to Dvl-1 PDZ. Our first interest was oriented towards sulfonamides. Hori et al (Hori 2018) have recently reported 3-({3-[(2-carboxyphenyl)sulfamoyl]phenyl}sulfamoyl)benzoic acid (NPL-1011) binding to Dvl-1 PDZ via the

detection of chemical shift changes, and further sulfonamide compounds that showed smaller effects, indicating weaker binding. We examined the binding constant of NPL-1011 which possesses two sulfonamide moieties by ITC and found a value of 79.7 ± 53.3 μM, see Table 2. For further comparisons, we assayed also CBC-322338/3289-8625, Sulindac and NSC668036 by ITC. Surprisingly, CBC-322338/3289-8625 showed very low affinity, with a K_D above 400 μM in our ITC assay, in line with the value found by Hori et al (Hori 2018) (954 +/- 403 μM). We also applied an NMR shift assay (Figure S8), yielding a ΔCSP around 0.1. Based on NMR and ITC studies, the binding affinity of CBC-322338/3289-8625 to DVL-3 seems to be less than 50 micromolar (comparing the CSPs from the NMR assay with those of our other compounds listed in Table S1 and the respective binding constants in Table 1, and considering also the weak heat development in our ITC assay) which was larger than the originally reported value (10.6 +/- 1.7) (Grandy 2009) that was obtained with a different method. Concerning non-sulfonamide compounds, a K_D of 8.3 ± 2.5 μM was detected for Sulindac, while NSC668036 (Shan 2005) did not show high-affinity binding. These results are largely in agreement with literature. In all cases, compounds were tested for purity after K_D measurements (see Supporting Information Figures S9A-D).

Selectivity testing using a set of selected PDZ domains

Compounds **18**, **20** and **21** were tested towards other PDZ domains for selectivity. The set included PSD95-PDZ 2 and 3, Shank-3, α-syntrophin, and AF-6 PDZ. According to the determined chemical shift perturbations (Supporting Information Table S4), our compounds show no or very weak interactions with the selected PDZ domains ($0.05 < \Delta CSP \leq 0.1$) ppm. These findings led to the conclusion that our compounds show considerable selectivity towards Dvl PDZ domains. This selectivity might be due to a unique feature of Dvl PDZ where R320 (Dvl-3 PDZ) or R322 (Dvl-1 PDZ) are crucial for interactions, explaining selectivity with respect to other PDZ domains. In addition, the large hydrophobic cavity for the side chain of the C-terminal residue of the interacting peptide is occupied by a large moiety in case of compounds **18**, **20** and **21** which might not be accommodated in most other PDZ domains.

Dvl inhibitors antagonize canonical Wnt signalling and Wnt-related properties of cancer cells

Taking advantage of a lentivirus that encodes GFP in a β-catenin/TCF-dependent fashion (TOP-GFP, SABiosciences), a stable HEK293 reporter cell line was established to evaluate the inhibitory effect of compounds **18**, **20** and **21** on canonical Wnt signalling activity. TOP-GFP expression in this cell line was induced by the ligand Wnt3a, which directly activates the Frizzled-Dishevelled complex and protects β-catenin from degradation by the destruction complex (Figure 2A). Remarkably, all three compounds inhibited Wnt signalling induced by Wnt3a in a dose-dependent manner (Figure 2B), yielding IC_{50} values between 50-80 μM.

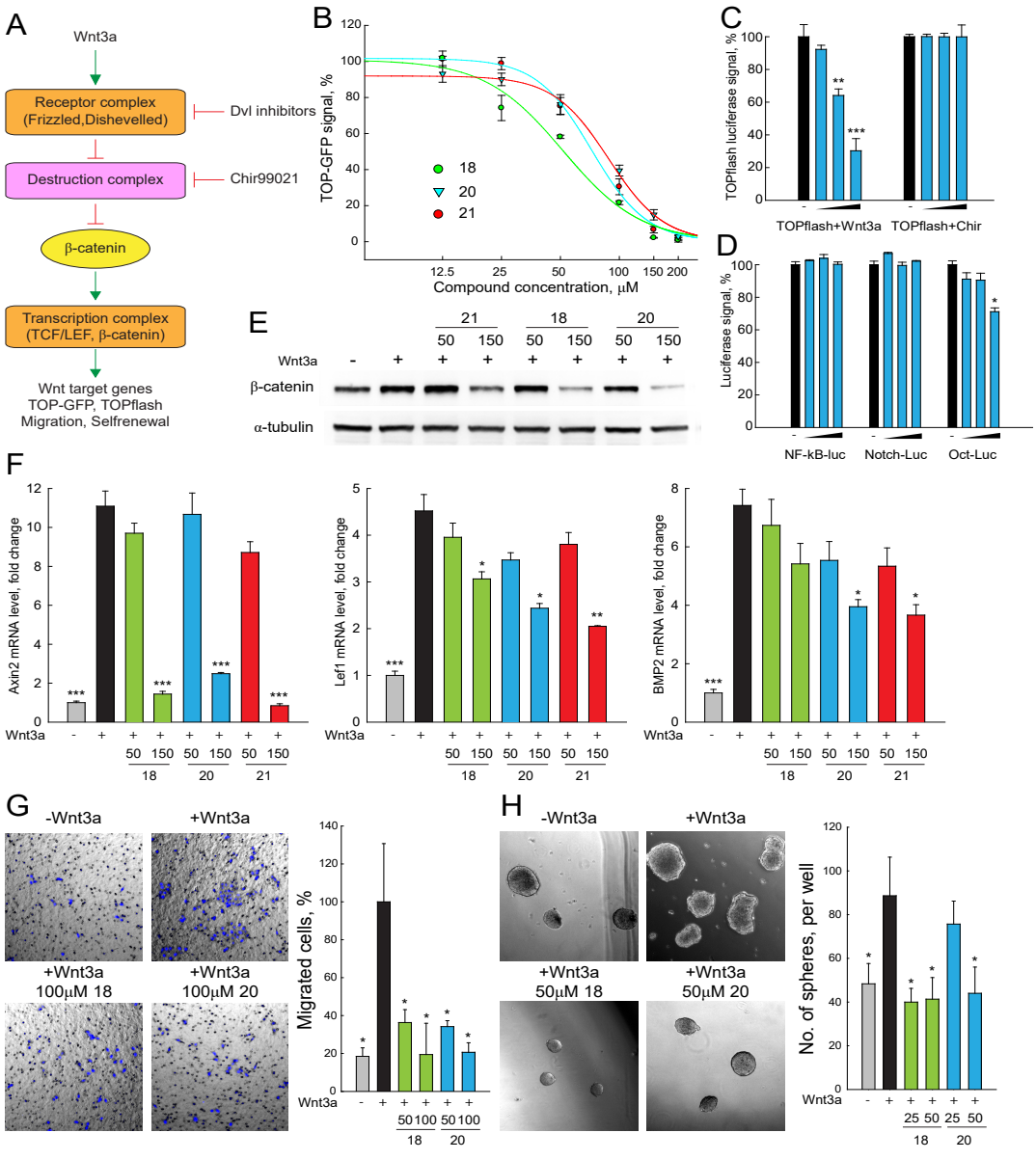

Figure 2

Figure 2. DVL inhibitors antagonize Wnt signalling and Wnt related properties of cancer cells induced by Wnt3a. A. Scheme of Wnt signalling pathway. Important components of the Wnt signalling pathway are schematically presented. Wnt3a treatment

increases the transcription of Wnt targets, enhances signals of TOP-GFP and TOPflash assays, and promotes Wnt related biological properties of cancer cells. **B.** TOP-GFP reporter assays were performed with HEK293 reporter cell line. Compound **18**, **20** and **21** inhibited Wnt3a induced Wnt activation in dose-dependent manner with IC_{50} of 50~75 μM. **C&D.** TOPflash assays stimulated with Chir99021 and reporter assays of other pathway were used to evaluate the specificity of compound **20**. Compound **20** specifically inhibited Wnt3a induced Wnt activation, and had no or mild effect on Chir99021 induced Wnt activation and other signalling pathways including NF-κB, Notch and Oct4. **E.** β-Catenin protein levels were detected with Western blotting in Hela cells. Compound **18**, **20** and **21** (150 μM) inhibited accumulation of β-catenin in Hela cells treated with Wnt3a. **F.** The mRNA levels of Wnt target genes (Axin2, Lef1 and Bmp2) in Hela cells were measured with quantitative real-time PCR. Compounds **18**, **20** and **21** (150 μM) reduced the transcription of Wnt target genes that are enhanced by Wnt3a treatment in Hela cells. **G.** Cell migration of SW480 cells after Wnt3a treatment was assessed by transwell assays. Compounds **18** and **20** (50~100 μM) reduced the migration of SW480 cells enhanced by Wnt3a. **H.** SW480 cells were cultured in serum-free non-adherent condition to evaluate the self-renewal property enhanced by Wnt3a treatment. Compound **18** and **20** (25~50 μM) reduced sphere formation of SW480 cells that was enhanced by Wnt3a treatment. For all tests, three independent biological replicas were performed and error bars represent standard deviations. P-values were calculated from T-test. *: $P < 0.05$; **: $P < 0.01$; ***: $P < 0.001$.

To further evaluate the specificity of our Dvl inhibitors, the conventional TOPflash (Molenaar 1996) and other luciferase reporter assays were performed. In Hela cells, **20** inhibited TOP-luciferase signals stimulated by Wnt3a but not by CHIR99021(Sineva 2010), a compound that activates Wnt signalling downstream of Dvl (Figure 2A, C). Compound **20** had no significant inhibitory effects in reporter assays that measure the activity of other signalling systems, e.g., NF-κB-luciferase stimulated by recombinant TNFα, Notch-luciferase stimulated by the overexpression of the Notch intracellular domain, or the Oct-luciferase assay that is stimulated by overexpression of Oct4 (SABiosciences, Figure 2D). These results strongly indicate that **20** is specific for canonical Wnt signalling at the upstream level.

Increased β-catenin protein level is a hallmark of active Wnt signalling (Kishida 1999). Once β-catenin is accumulated in the cytoplasm, it can translocate into the nucleus and activate the transcription of Wnt target genes by interacting with transcription factors of the TCF/LEF family (Figure 2A) (Behrens 1996). In Hela cells, all three Dvl inhibitors blocked the increase of production of β-catenin by Wnt3a in dose-dependent manners, as seen by Western blotting (Figure 2E). Increased mRNA levels of the Wnt target genes Axin2, Lef1 and Bmp2 (Riese 1997, Jho 2002, Lewis 2010) were induced by Wnt3a treatment, as measured by qRT-PCR, and these increases were reduced by compounds **18**, **20** and **21** (Figure 2F). These results demonstrate that compounds **18**, **20** and **21** inhibit Wnt signalling as indicated by reduced accumulation of β-catenin and low expression of typical Wnt target genes.

Canonical Wnt signalling contributes to cancer progression by inducing high motility and invasion of cancer cells while retaining the self-renewal property of cancer initiating cells (Fritzmann 2009, Sack 2011, Vermeulen 2010, Malanchi 2008). In particular, cancer initiating cells are propagated and enriched in non-adherent sphere culture, demonstrating the self-renewal capacity of the stem cells

(Kanwar 2010, Fan 2011). To investigate the potential value of the Dvl inhibitors for interfering with these Wnt-related properties of cancer cells, the subline SW480WL was derived from the SW480 colon cancer cell line, which exhibits a low level of endogenous Wnt activity (Fang 2012). The cell migration and self-renewal properties of SW480WL cells were enhanced by Wnt3a treatment, as revealed by transwell and sphere formation assays (Figure 2G, H). Compounds **18** and **20** prevented increased cell migration and sphere formation. These results indicate that our Dvl inhibitors may be developed into lead compounds that interfere with Wnt signalling.

CONCLUSIONS

In the present work, small molecules that bind to Dvl PDZ in the one-digit micromolar range with considerable selectivity have been developed by an extensive structure-based design approach. With regards to the affinity determined by ITC, compound **18** binds to Dvl-1 and Dvl-3 in vitro with K_D values of 2.4 and 9.4, respectively, comparing very well with known ligands. X-ray structures of Dvl-3 PDZ complexes with selected compounds provided insight into crucial interactions and served as the basis for the design of tight binding compounds with reduced toxicity. The structural investigations revealed that these compounds form hydrogen bonds with the amide groups of residues L260, G261 and I262 in the PDZ-domain loop and the side chains of residues H324 and R320. Finally, the chosen methodology, virtual screening followed by a two-stage NMR based screening, X-ray crystallography, and chemical synthesis is an excellent path towards bioactive interaction partners. Our best compounds effectively inhibited the canonical Wnt signalling pathway in a selective manner and could be developed for further studies.

Experimental Section

Clustering binding sites and selection of representative PDZ domains

Three-dimensional structures of PDZ domains were retrieved from the PDB (Berman 2000). At the time of the study from a total of 266 PDB files, 126 were NMR solution structures and 140 derived from X-ray diffraction studies. The structures belong to 163 PDZ domains of 117 different proteins from 11 organisms. Files which contain more than one 3D conformation for a domain (up to 50 for NMR-derived

data) were split into separate structures and considered independently. The total number of unique 3D structures was 2,708.

Amino acid sequences of PDZ domains were aligned using Clustal Omega software (Sievers 2011). Based on the alignment, for each structure, residues which form the binding site (strand βB and helix αB) were determined (Supporting Information Figure S8). The centre of the binding site was defined as a geometric centre of Cα atoms of 7 residues (6 residues from the βB strand and the second residue from the αB helix). Such bias toward the βB strand was made to cover sites occupied by residues in -1 and -3 positions.

The triangulated solvent accessible surface for each PDZ structure was built using MSMS software (Sanner 1996) with a spherical probe radius of 1.4 Å and vertex density 10 $Å^{-1}$. The largest connected set of surface vertices within 9 Å from the centre of the binding site was used to construct shape-based numerical descriptors. The descriptors are 508-dimensional vectors of non-negative integer numbers and were built using a shape distributions approach (Osada 2002). In total 10 (Pawson 2007) vertex triplets were selected randomly, each forming a triangle. Triangles which had a side longer than 16 Å were discarded. Triangle sides were distributed into 16 length bins, each 1 Å wide, covering lengths from 0 to 16 Å. A combination of three sorted side lengths, each belonging to one of 16 distance bins, defines one of 508 categories of the triangles. The number of triangles of each category was calculated, resulting in a 508-dimensional vector which is used as a numerical descriptor of the binding pocket shape. For further operations with descriptors, Euclidian metric was introduced. Shape descriptors were distributed into 6 clusters using k-means algorithm (Jain 1988). For each cluster, a centroid structure was defined as the one, whose descriptor is the closest to mean descriptor for the cluster. The centroid structures (2O2T#B.pdb, 1VA8#3.pdb, 2DLU#01.pdb, 1UHP#8.pdb, 2OS6#8.pdb, 3LNX#A.pdb) were used for docking.

PDZ targeted library design

Screening collection by Enamine Ltd. (Chuprina 2010) containing a total of 1,195,395 drug-like compounds was used as the primary source of small molecules. Natural ligand of PDZ is the C-terminus of a peptide with carboxylic group making extensive hydrogen bond network with the "ΦGΦ" motif.

Since the carboxyl provides either of negative charge and hydrogen bond acceptor, we want our ligands to retain at least one of these features. Therefore, we pre-filtered the stock library to bear chemical groups which have negatively charged and/or hydrogen bond acceptor functionality. In total 65,288 compounds were selected for the virtual screening study. The selected 6 centroids of PDZ domains and the prepared compound set were subjected to high-throughput docking using the QXP/Flo software (McMartin 1997). Complexes were generated with 100 steps of sdock + routine, and 10 conformations per complex were saved.

Processing of docking poses started with filtering by contact term *Cntc* from the QXP/Flo scoring function. Entries with Cntc < 45 were discarded, which removed complexes with weak geometries of bound ligands. The remained filtering was performed with the in-house MultiFilter program that allows flexible geometry-based filtering. We applied two algorithms, *nearest-atom* filter and *hydrogen-bond* filter. The former filters complexes by distance from a given protein atom to the nearest heavy ligand atom, while in the latter, filtering is based upon the number of hydrogen bonds calculated for a given complex geometry. With the *nearest-atom* routine we selected compounds that filled the P_0 pocket and sterically mimicked binding of a peptide carboxylic group. Peptide group hydrogens of the "ΦGΦ" motif and atoms forming the hydrophobic pocket were used for that. With the *hydrogen-bond* filter we selected compounds that formed extensive hydrogen bonding with the PDZ domain. Both these properties might have larger impact on binding rather than negative charge (Harris 2003). Details on atoms used for filtering and thresholds for *hydrogen-bond* filtering, as well as the resulting number of compounds, are provided in Supporting Information Table S5. Compounds from complexes which passed through these filters were incorporated into a targeted library for the PDZ-domain family. The final library contained 1119 compounds in total.

Screening of compounds

Two-dimensional ^{1}H-^{15}N HSQC spectra were used to screen a library of 212 compounds designed by the company Enamine for PDZ domains. 50 μM of ^{15}N-labeled protein samples were prepared in a 20 mM sodium phosphate buffer, containing 50 mM sodium chloride, 0.02% (w/v) NaN_3, at pH 7.4. Stock solutions of small molecules were prepared in DMSO-*d6* at a concentration of 160 mM. A ^{1}H-^{15}N HSQC

spectrum of Dvl PDZ was acquired at 300 K with 5% DMSO-*d6* in the absence of ligand as reference spectrum. Mixtures of 16 compounds were added to ^{15}N-labeled Dvl PDZ at 8-fold molar excess each. The final concentration of DMSO-*d6* in the protein-ligand solutions was 5%. Spectra were acquired with 8 scans and 256 points in the indirect dimension. Compound binding was deduced if the resonance position of a cross-peak was significantly shifted compared to the reference spectrum. The active compound was obtained through successive deconvolution. Experiments were recorded on a Bruker DRX600 spectrometer equipped with a triple-resonance cryoprobe. The preparation of samples was done automatically by a Tecan Genesis RSP 150 pipetting robot. Spectra were analysed using the programs TOPSPIN and SPARKY.[47]

Synthesis of compounds

All reagents and starting materials were purchased from Sigma-Aldrich Chemie GmbH, ABCR GmbH & Co.KG, alfa Aesar GmbH & Co.KG or Acros Organics and used without further purification. All air or moisture-sensitive reactions were carried out under dry nitrogen using standard Schlenk techniques. Solvents were removed by evaporation on a Heidolph Laborota 4000 with vacuum provided by a PC 3001 Vaccubrand pump. Thin-layer chromatography (TLC) was performed on plastic-backed plates pre-coated with silica gel 60 F_{254} (0.2 mm). Visualization was achieved under an ultraviolet (UV) lamp (254 and 366 nm). Flash chromatography was performed using J.T Baker silica gel 60 (30-63 µm). Analytical high-performance liquid chromatography (HPLC) was performed on a Shimadzu LC-20 (degasser DGU-20A3, controller CBM-20A, autosampler SIL-20A) with a DAD-UV detector (SPD-M20A), using a reverse-phase C18 column (Nucleodur 100-5, 5 µM, 250 mm x 4 mm, Macherey-Nagel, Düren, Germany). Separation of compounds by preparative HPLC was performed on a Shimadzu LC-8A system equipped with a UV detector (SPD-M20A), using a semi-preparative C18 column (Nucleodur 100-5, 5 µM, 250 mm x 10 mm, Macherey-Nagel) or preparative C18 column (Nucleodur 100-5, 5 µM, 250 mm x 21 mm, Macherey-Nagel). The detection wavelength was 254 nm. Gradients of acetonitrile-water with 0.1% TFA were used for elution at flow rates of 1 mL/min, 8 mL/min, and 14 mL/min on the analytical, semi-preparative and preparative columns respectively. Melting points (mp) were determined with Stuart Melting Point Apparatus SMP3 and are not corrected. Mass spectra were

recorded on a 4000Q TRAP LC/MS/MS/ System for AB Applied Biosystems MDS SCIEX. NMR spectra were recorded on a Bruker AV300 spectrometer instrument operating at 300 MHz for proton frequency using DMSO-*d6* solutions. Chemical shifts were quoted relative to the residual DMSO peak (^{1}H: δ = 2.50 ppm, ^{13}C: δ = 39.52 ppm). Coupling constants (J) are given in Hertz (Hz). Splitting patterns are indicated as follows: singlet (s), doublet (d), triplet (t), quartet (q), multiple (m), broad (b). Purity of each compound used for biological testing was ≥95% unless otherwise noted. The purity check of known inhibitors purchased for comparison with our compounds are found in Supporting Information Figure S9.

Synthesis of compounds 8, 11 – 17

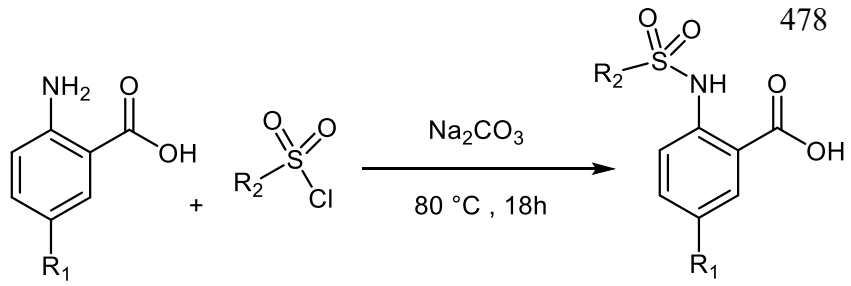

478

R_1 = CF_3 , Br, Cl

R_2 =

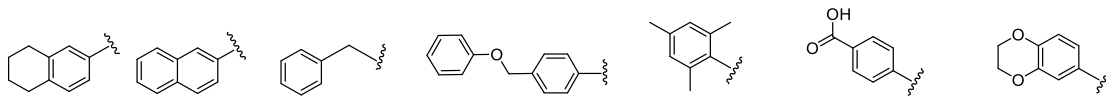

Scheme 3: Synthesis of compounds 8, 11 - 17

To a solution of anthranilic acid substituted with the appropriate R_1 (1.32 mmol) and sodium carbonate (3.17 mmol) in water (2 mL) at 80 °C, the sulfonyl chloride (1.58 mmol) substituted with the appropriate R_2 was added over a period of 5 minutes. The stirring continued for 18 h at 80 °C. The reaction mixture was cooled to room temperature and acidified with 6 N HCl, and the resulting solid precipitate was filtered, washed with water and dried to give the crude product. The final product was obtained by preparative HPLC (Puranik 2008).

2-(5,6,7,8-tetrahydronaphthalene-2-sulfonamido)- 5- (trifluoromethyl) benzoic acid (8)

(0.52 g, 74% yield) **^{1}H-NMR** (300 MHz, DMSO-d6): δ = 11.77 [s, 1H, CO*OH*], 8.13 [s, 1H, *NH*], 7.85 [d, $^{3}J_{6,4}$ = 2.1 Hz, 1H, 6-H_{Ar}] 7.62 [d, $^{4}J_{1',3'}$ = 2.1Hz , 1H , 1′-H_{Ar}] 7.53 [dd, $^{3}J_{4,3}$ = 7.1 Hz, $^{4}J_{4,6}$ = 2.1 Hz, 4-H_{Ar}] 7.36 [dd, $^{3}J_{3'4'}$ = 7.5 Hz, $^{4}J_{3',1'}$ = 2.4 Hz, 1H, 3′-H_{Ar}] 7.15 [d, $^{3}J_{4',3'}$ = 7.5Hz, 1H,4′-H_{Ar}] , 6.90 [d, $^{3}J_{3,4}$ = 7.1Hz, 1H , 3-H_{Ar}] 2.73 (m, 4H, CH_2); 1.6 (m, 4H, CH_2);-**^{13}C-NMR** (75 MHz, DMSO-d6): δ = 169.1(C, C_{Ar}-8], 152.7(C, C_{Ar}-2), 143.8 (C, C_{Ar}-4a′), 138.7(C, C_{Ar}-2′), 135.9 (C, C_{Ar}-8a′), 130.4(CH, C_{Ar}-4), 128.7 (CH, C_{Ar}-6), 127.5 (CH, C_{Ar}-1′), 124.0 (CH, C_{Ar}-4′), 121.6 (C, C-6), 118.2 (C, C_{Ar}-5), 116.9 (C, C_{Ar}-3), 29.0 (CH_2, C-8′), 28.8 (CH_2, C-5′), 22.3 (CH_2, C-6′), 22.2 (CH_2, C-7′); mp: 177°C; MS (ESI) *m*/z:calcd. for $C_{18}H_{16}F_3NO_4S$, 399; found 400 $[M+H]^+$.

5-bromo-2-(naphthalene-2-sulfonamido) benzoic acid (11)

(0.13 g, 67% yield) **^{1}H-NMR** (300 MHz, DMSO-d6): δ = 10.2 [s, 1H, *COOH*], 9.8 [s, 1H, *NH*] 8.59 [d, $^{4}J_{1',3'}$ = 1.4 Hz, 1 H, 1′-H_{Ar}], 8.17 [d, $^{3}J_{8',7'}$ = 7.8 Hz, 1 H, 8′-H_{Ar}], 8.10 [d, $^{3}J_{4'3'}$ = 8.8 Hz, 1 H, 4′-H_{Ar}], 8.02 [d, $^{3}J_{5',6'}$ = 7.8 Hz, 1 H, 5′-H_{Ar}], 7.93 [d, $^{4}J_{6,4}$ = 2.4 Hz, 1 H, 6-H_{Ar}], 7.77 [dd, $^{3}J_{3',4'}$ = 8.8 Hz, $^{4}J_{3',1'}$ = 1.4Hz ,1 H, 3′-H_{Ar}], 7.72 – 7.65 [m, 3 H, 4-H_{Ar}, 6′-H_{Ar}, 7′-H_{Ar}] , 7.51 [d, $^{3}J_{3,4}$ = 8.9 Hz, 1 H, 3-H_{Ar}]. – **^{13}C-NMR** (75 MHz, DMSO-d6): δ = 168.2 (C, C-7) ,138.8 (C, C_{Ar}-2),136.8 (CH, C_{Ar}-4),135.3 (C, C_{Ar}-4a′),134.4 (C, C_{Ar}-8a′) ,133.4 (CH, C_{Ar}-6) ,131.4 (CH, C_{Ar}-6′), 129.3 (CH, C_{Ar}-4′) ,128.5 (CH, C_{Ar}-8′),127.8 (2xCH, C_{Ar}-5′, C_{Ar}-7′) 121.6 (CH, C_{Ar}-3′),120.6 (CH, C_{Ar}-3),119.0(C, C_{Ar}-1) ,114.9 (C, C_{Ar}-5). Mp: 199°C; (ESI) *m*/z: calcd.for $C_{17}H_{11}BrNO_4S^-$; 403.9560: found 403.9613 $[M-H]^-$.

5-bromo-2-(phenylmethylsulfonamido)benzoic acid (12)

(0.07g, 42% yield) **^{1}H-NMR** (300 MHz, DMSO-d6): δ = 10.57 [s, 1 H, COO*H*], 8.05 [d, $^{4}J_{6,4}$ = 2.4 Hz, 1 H, 6-H_{Ar}], 7.75 [dd, $^{3}J_{4,3}$ = 8.9 Hz, $^{4}J_{4,6}$ = 2.4Hz ,1 H, H-4$_{Ar}$], 7.49 [d,$^{3}J_{3,4}$ = 8.9 Hz,1 H, 3-H_{Ar}], 7.33 – 7.28 [m, 3 H, 3′-H_{Ar} , 5′-H_{Ar}], 7.23 – 7.20 [m, 2 H, 4′-H_{Ar}], 5.75 [s, 1 H, N*H*], 4.72 [s, 2 H, 1′-H] **^{13}C-NMR** (75 MHz, DMSO-d6): δ = 168.3 (C, C-7) , 139.9 (C, C_{Ar}-2), 137(CH, C_{Ar}-4), 133.4 (CH, C_{Ar}-6), 130.7 (CH, C_{Ar}-3′) , 128.6 (C, C_{Ar}-2′) , 128.4 (CH, C_{Ar}-5′) , 128.3 (CH, C_{Ar}-4′) , 119.5 (CH, C_{Ar}-3) , 117.5 (C, C_{Ar}-1) , 113.9 (C, C_{Ar}-5) , 57.4 (CH_2, C-1′). Mp: 216°C; (ESI) *m*/z: calcd.for $C_{14}H_{11}BrNO_4S^-$ 367.9860; found 367.9878 $[M-H]^-$.

5-bromo-2-(4-(phenoxymethyl)phenylsulfonamido)benzoic acid (13)

(0.6 g, 29% yield) 1H-NMR (300 MHz, DMSO-d6): δ = 7.97 [d, $^{4}J_{6,4}$ = 2.4 Hz, 1 H, 6-H_{Ar}), 7.85 (d, $^{3}J_{2',3'}$ = 8.3 Hz, 2 H, 3′-H_{Ar}), 7.73 [dd, $^{3}J_{4,3}$ = 8.9 Hz, $^{4}J_{4,6}$ = 2.4Hz , 1 H,4-H_{Ar}], 7.63 [d, $^{3}J_{2',3'}$ = 8.3 Hz, 2

H, 2′-H_{Ar}], 7.47 [d, $^{3}J_{3,4}$ = 8.9 Hz, 1 H, 3-H_{Ar}], 7.29 [dd, $^{3}J_{3",2"} = {}^{3}J_{3",4"}$ =7.3 Hz, 2 H, 3"-H_{Ar}], 7.00 – 6.92 [m, 3 H, 4"-H_{Ar} , 2"-H_{Ar}], 5.17 [s, H, 5′-H]. − **13C-NMR** (75 MHz, DMSO-d6): δ = 168.2 (C, C-7) , 157.9 (C, C_{Ar}-1") , 143.2 (C, C_{Ar}-4′), 138.8 (C, C_{Ar}-2), 137.5 (C, C_{Ar}-1′) , 136.9 (CH, C_{Ar}-4) 133.5 (CH, C_{Ar}-6), 129.4(CH, C_{Ar}-3"), 128.1(CH, C_{Ar}-2′),127.0 (CH, C_{Ar}-3′) , 120.9 (CH, C_{Ar}-4") , 120.5 (CH, C_{Ar}-3) , 119.0 (C, C_{Ar}-1) , 114.9(CH, C_{Ar}-5), 114.7 (CH, C_{Ar}-2"), 68.0 (CH_2, C-5′) Mp: 175°C; (ESI) m/z: calcd for C20H15BrNO5S- 459.9860 found 459.9878 [M-H]-.

5-bromo-2-(2,4,6-trimethylphenylsulfoamido)benzoic acid (14)

(0.6 g, 78% yield) **^{1}H-NMR** (300 MHz, DMSO-d_6): δ = 11.77 [s,1H, *COOH*], 9.98 [s, 1H, *NH*], 7.68 [d, $^{3}J_{6,4}$ = 7.4 Hz, 1H, 6-H_{Ar}], 7.51[dd, $^{3}J_{4,3}$ =7.1Hz, $^{4}J_{4,6}$ =7.4 Hz, 1H 4-H_{Ar}], 7.17 [d, 2H, 4′-H_{Ar} , 6′-H_{Ar}], 7.14 [d, $^{3}J_{3,4}$= 1H,3-H_{Ar}] , 2.56 [s, 6H, CH_3, 9′-H, 7′-H], 2.21 [s, 3H, CH_3, 8′-H];-**^{13}C-NMR** (300 MHz, DMSO-d_6): δ = 168.8 (C, C-7), 143.3 (C, C_{Ar}-2), 139.5 (C, C_{Ar}-2′), 139.0 and 139.0 (2xC, C_{Ar}-3′, C_{Ar}-1′) 137.3 (CH, C_{Ar}-4), 134.0 (CH, C_{Ar}-6′), 133.0 (CH, C_{Ar}-6), 132.5 and 132.5 (2XCH, C_{Ar}-4′, C_{Ar}-6′) 119.1(CH, C_{Ar}-3), 117.9(C, C_{Ar}-5), 114.3 (C, C_{Ar}-1), 22.5 and 22.5 (2 x CH_3, C-7′, C-9′) 20.7 (CH_3, C-8′) ; mp: 185; MS (ESI): m/z 399 [M+H]+.

2-(4-acetylphenylsulfoamido)-5-(trifluoromethyl)benzoic acid (15)

(0.4 g, 63% yield) **^{1}H-NMR** (300 MHz, DMSO-d6): δ = 12.28 [s, 1H, *COOH*]; 12.10 [s, 1H, *NH*], 8.11 [d, $^{4}J_{6,4}$= 2.5 Hz, 1H, 6-H_{Ar}], 8.08 [d, $^{3}J_{3'2'}$ = 7.5 Hz, 2H, 3′-H_{Ar}], 7.86 [dd, $^{4}J_{4,6}$ = 2.5 Hz, $^{3}J_{4,3}$ = 7.3Hz, 1H, 4-H_{Ar}], 7.64 [d, $^{3}J_{4,3}$ = 7.3 Hz, 1H, 3-H_{Ar}] , 7.56 [dd $^{3}J_{2',3'}$ = 7.5Hz, $^{4}J_{2',6'}$ =2.3Hz, 2H, 2′-H_{Ar}, 6′-H_{Ar}] 7.22 [dd , $^{3}J_{3',2'}$ = 7.5Hz , $^{4}J_{3',5'}$ = 2.1Hz , 2H, 3′-H_{Ar}, 5′-H_{Ar}] 2.50 [s, 3H, CH_3, 8′-H]; - **^{13}C-NMR** (75 MHz, DMSO-d6): δ = 197.9 (C, C-7′), 169.1(C, C-8), 151.8 (C, C_{Ar}-2) 143.5 (C, C_{Ar}-1′), 142.5 (C, C_{Ar}-4′), 140.6 (CH, C_{Ar}-4), 131.4 (CH, C_{Ar}-7), 129.6 (2XCH, C_{Ar}-3′, C_{Ar}-5′), 128.6 (2xCH, C_{Ar}-2′, C_{Ar}-6′), 127.6 (C, C_{Ar}-6), 123.0 (C, C-$_{Ar}$-5), 118.7 (CH, C_{Ar}-3), 27.3 (CH_3, C-8′); mp: 170°C; MS (ESI) *m*/z : calcd. for $C_{16}H_{12}F_3NO_5S$. 387; found 388 $[M+H]^+$.

2-(2,3-dihydrobenzo[*b*][1,4]dioxine-6-sulfonamido)-5-(trifluoromethyl)benzoic acid (16)

(0.4 g, 65% yield) **^{1}H-NMR** (300 MHz, DMSO-d6): δ = 11.48 [s, 1H, *COOH*], 8.13[s, 1H, *NH*] , 7.89 [d, $^{4}J_{6,4}$ = 3,9 Hz , 1H , 6-H_{Ar}] 7.66 [dd, $^{3}J_{4,3}$ = 7.2 Hz, $^{4}J_{4,6}$ = 4.3 Hz, 1H, 4-H_{Ar}], 7.23 [d, $^{3}J_{4,3}$ = 7,2 Hz 1H, 3-H_{Ar}], 7.11 [dd, $^{3}J_{2',3'}$ = 7.3Hz , $^{4}J_{2',8'}$= 3.2Hz , 1H, 2′-HAr] 6.95 [d, $^{4}J_{2',8'}$= 3.2 Hz, 1H , 8′-H_{Ar}] 4.23 – 4.31 [m, 4H, 5′-H, 6′-H]; - **^{13}C-NMR** (75-MHz, DMSO-d6): δ = 168.9(C,

C-8), 148.3(C, C-4′), 143.8 (C, C-2), 143.5 (C, C-7′) , 131.3 (C, C-1′), 130.8 (CH, C-4), 128.6(CH, C-6), 125.7 (C, C-7), 122.1(C, C-5), 120.9(CH, C-2′), 118.3 (CH, C-3), 118.1(CH, C-3′), 116.8 (CH, C-8′) , 64.7(CH_2, C-5′) 64.3 (CH_2, C-6′); mp: 178°C; MS (ESI) *m*/z: calcd. for $C_{16}H_{12}F_3NO_6S$. 403; found 404 $[M+H]^+$.

5-(trifluoromethyl)-2-(2,4,6-trimethylphenylsulfoamido)benzoic acid (17)

(0.38 g, 62% yield) **^{1}H-NMR** (300 MHz, DMSO-d6): δ = 12.28 [s, 1H, *COOH*], 11.60 [s, 1H, *NH*], 8.15 [d, $^4J_{6,4}$ = 4.3 Hz, 1H, 6-H_{Ar}] 7.92 [dd, $^3J_{4,3}$ =7.9 Hz, $^4J_{4,6}$= 2.1 Hz, 1H,4-H_{Ar}] 7.87 [d, $^4J_{6',4'}$= 1.9 Hz, 2H, 4′-H_{Ar} , 6′-H_{Ar}], 7.48 [d, $^3J_{3,4}$ = 7.9 Hz, 1H, 3-H_{Ar}] , 2.60 [s, 6H, CH_3 , 9′-H, 7′-H], 2.23 [s, 3H, CH_3, 8′-H]; - **^{13}C-NMR** (75 MHz, DMSO-d6): δ = 169.3 (C, C-7), 154.2 (C, C-2), 143.6 (C, C-2′) , 139.1 and 139.1 (2xC, C-1′, C-3′) 132.9 (C, C-5′), 132.5 (CH, C-4), 131.5 and 131.5 (2xCH, C-4′, C-6′) , 130.1(CH, C-6), 128.7 (C, C-8), 122.5 (C, C-5), 117.0 (CH, C-3), 109.0 (C, C-1) ,22.4 and 22.4 (2xCH_3,C-7′, C-9′), 20.8 (CH_3, C-8′) ; mp:184°C; MS (ESI) *m*/z: calcd. for $C_{17}H_{16}F_3NO_4S$; 387: found 388 $[M+H]^+$.

18, 19, 20, and **21** were purchased from Enamine, Kiev, Ukraine as pure compounds (see also Table S6, Supporting Information).

Determination of ligand binding and binding constant by NMR

50 μM of ^{15}N-labeled protein samples were prepared in a 20 mM sodium phosphate buffer containing 50 mM sodium chloride, 0.02 % (w/v) NaN_3, at pH 7.4. Stock solutions of small molecules were prepared in DMSO-*d6* at a concentration of 160 mM. A ^{1}H-^{15}N HSQC spectrum of Dvl PDZ was acquired at 300 K with 5% DMSO-*d6* in the absence of ligand as reference spectrum. Mixtures of 16 compounds were added to ^{15}N-labeled Dvl PDZ at 8-fold molar excess each. The final concentration of DMSO-*d6* in the protein-ligand solutions was 5%. Spectra were acquired with 8 scans and 256 points in the indirect dimension.

Binding was deduced if the resonance position of a cross-peak was significantly shifted compared to the reference spectrum. The active compound was obtained through successive deconvolution. Experiments were recorded on a Bruker DRX600 spectrometer equipped with a triple-resonance cryoprobe. The

preparation of samples was done automatically by a Tecan Genesis RSP 150 pipetting robot. Spectra were analysed using the programs TOPSPIN and SPARKY.

Chemical shift perturbations were obtained by comparing the ^{1}H-^{15}N backbone resonances of protein alone to those of protein-ligand complex. The mean shift difference (Δδ in ppm) was calculated using the equation 1 (Garrett 1997, Bertini 2011).

$$\Delta\delta = \sqrt{\frac{[\Delta\delta_H]^2 + [\Delta\delta_N/5]^2}{2}} \qquad (Eq.1)$$

Here $\Delta\delta_N$ and $\Delta\delta_H$ are the amide nitrogen and amide proton chemical shift differences between the free and the bound states of the protein. In order to estimate binding constants, titration experiments monitored by NMR were done. A series of ^{1}H-^{15}N HSQC were recorded as a function of ligand concentration. Residues showing a continuous chemical shift change and for which the intensity remained strong were classified as being in fast exchange. The dissociation binding constant was estimated by fitting the observed chemical shift change to equation 2 (Shuker 1996, Hajduk 1997).

$$\frac{\Delta\delta}{\Delta\delta_{max}} = \frac{([L_T] + [P_T] + K_D) - \sqrt{([L_T] + [P_T] + K_D)^2 - 4[L_T] \cdot [P_T]}}{2[P_T]} (Eq.2)$$

Δδ is the observed protein amide chemical shift change at a given compound concentration and $\Delta\delta_{max}$ the maximum chemical shift change at saturation. $[L_T]$ the total concentration of the compound, and $[P_T]$ the total concentration of the protein. K_D is the equilibrium dissociation constant. The K_D values are reported as means ± standard deviations of at least six residues influenced upon binding of the ligand.

Determination of binding constant by Isothermal Titration Calorimetry (ITC)

Isothermal Titration Calorimetry (ITC) experiments were performed using a VP-ITC system (MicroCal). Protein in 20 mM Hepes buffer, 50 mM NaCl, pH 7.4, was centrifuged and degassed before the experiment. A 200 µM ligand solution containing 2% DMSO was injected 30 times in 10 µL aliquots at 120 s intervals with a stirring speed of 1000 rpm into a 1.4 mL sample cell containing the Dvl PDZ

599 domain at a concentration of 20 μM at 25 °C. Control experiment was initially determined by titrating
600 ligand into buffer at same conditions. Titration of ligand into buffer yielded negligible heats.
601 Thermodynamic properties and binding constants were determined by fitting the data with a nonlinear
602 least-squares routine using a single-site binding model with Origin for ITC v.7.2 (Microcal).
603
604 **Protein expression**
605 PDZ domains of human AF6 (P55196-2, residues 985–1086) and murine α1-syntrophin (Q61234,
606 residues 81–164) were cloned into pGEX-6P-2 (Amersham Biosciences, Freiburg, Germany) and
607 pGAT2 (European Molecular Biology Laboratory, Heidelberg, Germany), respectively. Proteins were
608 expressed in *E. coli* BL21 (DE3) cells and purified as previously described (Boisguerin 2004). For the
609 cloning of the Dvl-1 PDZ domain (O14640, residues 245–338), IMAGp958J151157Q (ImaGenes) was
610 used as template. V250 is exchanged to isoleucine as in human Dvl-3 or murine Dvl-1. The C-terminal
611 C338 of the domain was exchanged by serine. Via cloning in pET46EK/LIC, a coding sequence for a
612 TEV (Tobacco Etch Virus) protease cleavage site was introduced. The resulting plasmid pDVL1 was
613 transformed in *E. coli* BL21 (DE3). Expression on two-fold M9 minimal medium with 0.5 g/L ^{15}N
614 NH_4Cl as sole nitrogen source in shaking culture was done at 25 °C overnight with 1 mM IPTG. A yield
615 of 25 mg of pure Dvl-1 was obtained from 1 L culture after IMAC, TEV protease cleavage, a second
616 IMAC, and gel filtration (Superdex 75). The protein domain Dvl-1_245–338 was supplied for NMR in
617 20 mM phosphate buffer, pH 7.4, 50 mM NaCl.
618 The production of Dvl-3 (Q92997 residues 243-336), mShank3 (Q4ACU6, residues 637-744) PDZ
619 domains and the 3 PDZ domains of PSD95 was described by Saupe et al (Saupe 2011).
620
621 **Crystallization and X-ray diffraction**
622 The His-tagged cleaved human Dvl-3 PDZ domain was concentrated to 12-20 mg/mL in the presence
623 of a 5-fold molar excess of compound **3**, **5**, **6**, **7**, **11** and **12**. Crystals of all complexes were grown at
624 room temperature by the sitting drop vapour-diffusion method. 200 nL Dvl-3/compound solution was
625 mixed with an equal volume of reservoir solution using the Gryphon (Formulatrix) pipetting robot.
626 Crystals of all complexes were grown to their final size within 4 to 14 days. The Dvl-3 PDZ domain

crystallized in complex with compound **3**and **7** in crystallization condition 30% PEG 8000, 0.2 M ammonium sulphate, 0.1 M MES pH 6.5; with compound **5** in 30% PEG 8000, 0.1 M MES pH 5.5; with compound **6** in 1.2 M ammonium sulphate, 0.1 M citric acid pH 5.0; with compound **12** in 32% PEG 8000, 0.2 M ammonium sulphate, 0.1 M Na-cacodylate pH 6.0; with compound **11** in 1 M ammonium sulphate, 1% PEG 3350, 0.1 M Bis-Tris pH 5.5; with compound **12** in 1.26 M sodium phosphate, 0.14 M potassium phosphate and with compound **18** in 1.5 M ammonium sulphate, 12% glycerol, 0.1 M Tris-HCl pH 8.5. The crystals were cryoprotected if necessary, for data collection by soaking for few seconds in precipitant solution containing 20% (v/v) glycerol and subsequently frozen in liquid nitrogen. Diffraction data were collected at 100 K at beamline BL14.1 at the synchrotron-radiation source BESSY, Helmholtz-Zentrum Berlin and processed with XDS.

Structure determination and refinement

Phases for the Dvl-3 PDZ domain in complex with compound 3 were obtained by molecular replacement with PHASER (McCoy 2007) using the *Xenopus laevis* Dishevelled PDZ domain structure (PDB code 2F0A) as a starting model. The reasonable crystal packing and electron density allowed further model and compound building using the program COOT (Emsley 2004) with iterative refinement with REFMAC (Murshudov 1997). All further complex structures were obtained in the same way but using the final refined compound free Dvl-3-PDZ structure as model for molecular replacement. The Ramachandran statistics were analysed by Molprobity (Chen 2010) for all complexes and all crystallographic statistics are given in Supporting Information Tables S2 and S3. Figures were prepared with PyMol. Atomic coordinates and structure factor amplitudes for DVL-3 PDZ domain in complex with compound **3**, **5**, **6**, **7**, **11**, **12**, **18** were deposited in the Protein Data Bank with accession codes 6ZBQ, 6ZBZ, 6ZC3, 6ZC4, 6ZC6, 6ZC7 and 6ZC8, respectively.

MTT assay

HEK293 cells were plated on a 96-well plate and treated with different concentrations of Dvl inhibitors. After 24 h treatment, 20 µl of MTT solution (5 mg/mL) was added into each well. After 2 h incubation,

cell culture medium was replaced with 50 μL DMSO, and the signal of the purple formazan, produced by living cells, was measured by a plate reader.

TOP-GFP reporter assay

The lentivirus particle (CCS-018L, SABiosciences) encoding GFP under the control of a basal promoter element (TATA box) joined to tandem repeats of a consensus TCF/LEF binding site was transfected into HEK293 cells. Stable cells were selected by puromycin (2 μg/mL) treatment. Wnt signalling activity indicated by GFP intensity was measured by flow cytometry after 24 h incubation with recombinant mouse Wnt3a (100 ng/mL) or GSK3 inhibitor CHIR99021 (3 μM) in the presence of Dvl inhibitors.

Luciferase reporter assays

Plasmids encoding a firefly luciferase reporter gene under the control of different responsive elements were transfected into Hela cells with a pRL-SV40 normalization reporter plasmid using the Lipofectamine 2000 (Invitrogen). After desired treatment, cells were harvested in the passive lysis buffer (Promega), and 15 μL cell lysate were transferred to 96-well LumiNunc plates (Thermo Scientific). Firefly luciferase and Renilla luciferase were detected with the D-luciferin buffer (75 mM Hepes, 4 mM $MgSO_4$, 20 mM DTT, 100 μM EDTA, 0.5 mM ATP, 135 μM Coenzyme A and 100 μM D-Luciferin sodium salt, pH 8.0) and the coelenterazine buffer (15 mM Na4PPi, 7.5 mM NaAc, 10 mM CDTA, 400 mM Na_2SO_4, 25 μM APMBT and 1.1 μM coelenterazine, pH 5.0) respectively using the CentroXS LB960 lumiometer (Berthold Technologies).

Immunoblotting

To assess the β-catenin accumulation in Hela cells, cells were treated with Wnt3a in the presence of Dvl inhibitors for 24 h and lysed in RIPA buffer (50 mM Tris, pH 8.0, 1% NP-40, 0.5% deoxycholate, 0.1% SDS, 150 mM NaCl). Equal amounts of protein were loaded on a SDS-PAGE. Separated proteins were blotted onto PVDF membranes for immunoblot analysis using anti-β-catenin antibody (610154, BD). HRP-conjugated anti-mouse antibody (715-035-150, Jackson ImmunoResearch laboratories) was used

for secondary detection with Western lightning chemiluminescence reagent plus (PerkinElmer) and Vilber Lourmat imaging system SL-3.

qRT-PCR analysis

To measure the Wnt target accumulation at mRNA level, Hela cells were treated with Wnt3a in the presence of Dvl inhibitors for 24 h. mRNA was extracted according to the standard TRIzol® protocol (Invitrogen) and reverse-transcribed using random primers (Invitrogen) and M-MLV reverse transcriptase (Promega). The qRT-PCR was performed in iQ5 Multicolor Real-Time PCR Detection System (Bio-Rad) using SYBR® Green (Thermo Scientific) and gene-specific primer pairs of Bmp2, Axin2, Lef1 and β-actin (endogenous control).

Migration assay

Cell motility was assessed using 24-well transwell (pore diameter: 8 μm, Corning). SW480WL cells were seeded in the upper chamber in serum free DMEM with 0.1% BSA; 20% serum was supplemented to medium in the lower chamber. After incubation with Wnt3a in the presence of Dvl inhibitors for 24 h, nonmigrant cells were scraped off using a cotton swab; the migrated cells on the filters were stained with DAPI, photographed and counted.

Colon sphere culture

SW480WL cells were trypsinised into single cells, seeded on 24-well cell culture plates precoated with 250 μl polyhema (12 mg/mL in 95% ethanol, Sigma) per well, and incubated with Wnt3a in the presence of Dvl inhibitors in the sphere culture medium (F12 : DMEM 1 : 1, 1X B-27 supplement, 20 ng/mL EGF, 20 ng/mL FGF, 0.5% methylcellulose) for 10 days. Numbers of spheres were then counted under the microscope.

Notes

The authors declare no competing financial interest.

ACKNOWLEDGEMENTS

This research was supported by the Deutsche Forschungsgemeinschaft (DFG) Research Group 806 and the EU-project iNext (Infrastructure for NMR, EM and X-rays for Translational Research, GA 653706). We thank M. Leidert and S. Radetzki for protein preparation, and B. Schlegel for NMR assistance. We also thank E. Specker for compound analysis.

ABBREVIATIONS USED

NMR, nuclear magnetic resonance; HSQC, Heteronuclear Single Quantum Correlation;
AU, asymmetric unit; SAR, derive structure activity relationships; vdW, van der Waals;
ITC, Isothermal titration calorimetry; PDZ, PSD95/Disc large/Zonula occludens 1);
Dvl, Dishevelled; PPI, protein-protein interactions; PDB, Protein Data Bank;
CSP, chemical shift perturbation; GFP, green fluorescent protein; DMSO, dimethyl sulfoxide;
PEG, polyethylene glycol; RNA, ribonucleic acid; mRNA, messenger RNA;
qRT-PCR, quantitative real-time polymerase chain reaction; DMEM Dulbecco's modified Eagle's medium ; BSA, bovine serum albumin;

ASSOCIATED CONTENT

Accession Codes

Atomic coordinates and structure factor amplitudes for DVL3 PDZ domain in complex with compound **3**, **5**, **6**, **7**, **11**, **12**, **18** were deposited in the Protein Data Bank with accession codes 6ZBQ, 6ZBZ, 6ZC3, 6ZC4, 6ZC6, 6ZC7 and 6ZC8, respectively. Authors will release the atomic coordinates and experimental data upon article publication.

Supporting information

1. Structure-based alignment of the amino acid sequences of Dvl-1,2,3 PDZ ; PSD95-PDZ-1,2,3 ; Af-6 and Syn PDZ domains. (S.2)

2. 1H-15N HSQC spectra of Dvl-3 PDZ domain alone and in the presence of varying concentrations of compound 3. (S.3)

738 **3.** Detailed views of diverse compounds bound to the Dvl-3 PDZ domain. (S.4)

739 **4.** Cell viability assays of compounds 3, 7,8, 9, 10, (A) and 18, 20, 21 (B). (S.5)

740 **5.** ITC binding assays of compound 18 with Dvl-3 PDZ (A) and with Dvl-1 PDZ (B). (S.5)

741 **6.** Structures of selected compounds used for comparison to our compounds. (S.6)

742 **7.** ITC data of selected compounds used for comparison to our compounds. (S.7)

743 **8.** NMR binding assay with compound 322338/3289-8625. (S.8)

744 **9.** Purity check of compounds. (S.9)

745 – Purity check of NPL-1011 compound. (S.9)

746 – Purity check of Sulindac compound. (S.10)

747 – Purity check of CalBioChem-322338 compound. (S.11)

748 – Purity check of NSC668036 compound. (S.12)

749 – LCMS of intermediate compound 8. (S.13)

750 – LCMS of intermediate compound 14. (S.13)

751 **10.** Chemical shift perturbation values of Dvl-3 PDZ and Dvl-1 PDZ for compounds (3-21). (S.14)

752 **11.** Data collection and refinement statistics of compounds 3, 5, 6, 7. (S.15)

753 **12.** Data collection and refinement statistics of compounds 11, 12, 18. (S.16)

754 **13.** Selectivity of ligands derived from chemical shift perturbation of compounds tested at other PDZ

755 domains. (S.17)

756 **14.** Details of Multifilter routines. (S.17)

757 **15.** Smiles codes and Compounds ID. (S.18)

758 **16.** NMR characterization of synthesized compounds (8, 11, 13, 14, 15, 16, 17). (S.21)

759

760 **References**

761 Behrens, J., von Kries, J. P., Kühl, M., Bruhn, L., Wedlich, D., Grosschedl, R. and Birchmeier,W.:
762 Functional interaction of beta-catenin with the transcription factor LEF-1. Nature, 382, 638-642,
763 DOI: 10.1038/382638a0, 1996.
764 Bertini, I., Chevanace, S., Del Conte, R., Lalli, D. and Turano, P.: The anti-apoptotic Bcl-x(L) protein,
765 a new piece in the puzzle of cytochrome c interactome. PLos One, 6:e18329, DOI:
766 10.1371/journal.pone.0018329, 2001.
767 Berman, H. M., Westbrook, J., Feng, Z., Gilliland, G., Bhat, T. N., Weissig, H., Shindyalov, I. N. and
768 Bourne, P.E.: The protein data bank, Nucleic. Acids Res., 28, 235 – 242, DOI: 10.1093/nar/28.1.235,
769 2000.

Boisguerin, P., Leben, R., Ay, B., Radziwill, G., Moelling, K., Dong, L. and Volkmer-Engert, R.: An improved method for the synthesis of cellulose membrane-bound peptides with free C termini is useful for PDZ domain binding studies. Chem. Biol., 11, 449 – 459, DOI: 10.1016/j.chembiol.2004.03.010, 2004.

Bui, T. D., Beier, D. R., Jonssen, M., Smith, K., Dorrington, S. M., Kaklamanis, L., Kearney, L., Regan, R., Sussman, D. J. and Harris, A. L.: cDNA cloning of a human dishevelled DVL-3 gene, mapping to 3q27, and expression in humanbreast and colon carcinomas. Biochem. Biophys. Res. Commun., 239, 510 – 516, DOI: 10.1006/bbrc.1997.7500, 1997.

Chandanamali, P., Antonio, M. F., Robert, C., Patrick, R. and Naoaki, F.: Sequence and subtype specificity in the high-affinity interaction between human frizzled and dishevelled proteins, Protein Sci., 18, 994 – 1002, DOI: 10.1002/pro.109, 2009.

Chen V. B., Arendall, W. B. 3rd; Headd, J. J. and Keedy, D. A., Immormino, R. M., Karpral, G. J., Murray, L. W., Richardson, J. S., Richardson, D. C.: MolProbity: all-atom structure validation for macromolecular crystallography. Acta Cryst., 66, 12 - 21, DOI: 10.1107/S0907444909042073, 2010.

Choi, J., Ma, S.; Kim, H.-Y., Yun, J.-H., Heo, J.-N., Lee, W., Choi, K.-Y. and No, K.: Identification of small-molecule compounds targeting the dishevelled PDZ domain by virtual screening and binding studies. Bioorg. Med. Chem., 24,3259–3266. Doi: 10.1016/j.bmc.2016.03.026, 2016.

Christensen, N. R., De Luca, M., Lever, M. B., Richner, M., Hansen, A. B., Noes-Holt, G., Jensen, K. L., Rathje, M., Jensen, D. B., Erlendsson, S., Bartling, C. R., Ammendrup-Johnsen, I., Pedersen, S. E., Schönauer, M., Nissen, K. B., Midtgaard, S. R., Teilum, K., Arleth, L., Sørensen, A. T., Bach, A., Strømgaard, K., Meehan, C. F., Vaegter, C. B., Gether, U. and Madsen, K. L.: A high-affinity, bivalent PDZ domain inhibitor complexes PICK1 to alleviate neuropathic pain. EMBO Mol. Med., 12 :e11248, Doi: 10.15252/emmm.201911248, 2020.

Christensen, N. R., Calyseva, J., Fernandes, E. F. A., et al.: PDZ Domains as Drug Targets. Adv. Ther., 2(7), 1800143, Doi:10.1002/adtp.201800143, 2019.

Chuprina, A., Lukin, O., Demoiseaux, R., Buzko, A. and Shivanyuk, A.: Drug- and lead-likeness, target class, and molecular diversity analysis of 7.9 million commercially available organic compounds provided by 29 suppliers. J. Chem. Inf. Model., 50, 470 - 499. Doi: 10.1021/ci900464s, 2010.

Doyle, D. A., Lee, A., Lewis, J., Kim, E., Sheng, M. and MacKinnon, R.: Crystal structures of a complexed and peptide-free membrane protein-binding domain: Molecular basis of peptide recognition by PDZ. Cell, 85, 1067-1076, DOI: 10.1016/s0092-8674(00)81307-0, 1996.

Emsley, P. and Cowtan, K.: Coot: model-building tools for molecular graphics. Acta Cryst., 60, 2126 – 2132 , DOI: 10.1107/S0907444904019158, 2004.

Fan, X., Quyang, N., Teng, H. and Yao, H.: Isolation and characterization of spheroid cells from the HT29 colon cancer cell line. Int. J. Colorect. Dis., 26, 1279 - 1285, DOI: 10.1007/s00384-011-1248-y, 2011.

Fang, L., Von Kries, J. P. and Birchmeier, W.: Identification of small-molecule antagonists of the TCF/β-catenin protein complex, in 30 years of Wnt signalling. EMBO Conference: Egmond aan Zee, Netherlands. p. 101, 2012.

Fanning, A. S. and Anderson, J. M.: Protein-protein interactions: PDZ domain networks. Curr. Biol., 6, 1385 – 1388, DOI: 10.1016/s0960-9822(96)00737-3, 1996.

Fritzmann, J., Morkel. M., Besser, D., Budczies, J., Kosel, F., Brembeck, F. H., Stein, U., Fichtner, I., Schlag, P. M. and Birchmeier, W.: A colorectal cancer expression profile that includes transforming growth factor beta inhibitor BAMBI predicts metastatic potential. Gastroenterology, 137, 165 - 175, DOI: 10.1053/j.gastro.2009.03.041, 2009.

Fujii, N., You, L., Xu, Z., Uematsu, K., Shan, J., He, B., Mikami, I., Edmondson, L.R., Neale, G., Zheng, J., Guy, R. K. and Jablons, D. M.: An antagonist of dishevelled protein-protein interaction suppresses β-catenin-dependent tumor cell growth. Cancer Res., 67, 573 - 579, DOI: 10.1158/0008-5472.CAN-06-2726, 2007.

Garrett, D. S., Seok Y. J., Peterkofsky A. and Gronenborn, A. M.: Identification by NMR of the binding surface for the histidine-containing phosphocarrier protein HPr on the N-terminal domain of enzyme I of the Escherichia coli phosphotransferase system. Biochem., 36, 4393 – 4398, DOI: 10.1021/bi970221q, 1997.

Goddard, T. D. and Kneller, D. G.: SPARKY 3, University of California, San Francisco, 2003.

825 Grandy, D., Shan, J., Zhang, X., Rao, S., Akunuru, S., Li, H., Zhang, Y., Alpatov, I., Zhang, X., Lang,
826 R., Shi, De-Li. and Zheng, J.: Discovery and characterization of a small molecule inhibitor of the
827 PDZ domain of dishevelled. J. Biol. Chem., 284, 16256–16263. DOI: 10.1074/jbc.M109.00 9647,
828 2009.
829 Hajduk, P. J., Sheppard, G., Nettesheim, D. G., Olejniczak, E. T., Shuker, S. B., Meadows, R. P.,
830 Steinman, D. H., Carrera, G. M. Jr., Marcotte, P. A., Severin, J., Walter, K., Smith, H., Gubbins, E.,
831 Simmer, R., Holzman, T. F., Morgan, D. W., Davidsen, S. K., Summers, J. B. and Fesik, S. W.:
832 Discovery of Potent Nonpeptide Inhibitors of Stromelysin Using SAR by NMR. J. Am. Chem. Soc.,
833 119, 5818 – 5827, DOI: 10.1021/ja9702778, 1997.
834 Hammond, M.C, Harris, B. Z., Lim, W. A., Bartlett, P. A.: β Strand Peptidomimetics as Potent PDZ
835 Domain Ligands. Chem. Biol., 13(12), 1247-1251, DOI: 10.1016/j.chembiol.2006.11.010, 2006.
836 Harris, B. Z., Lau, F. W., Fujii ,N., Guy, R. K. and Lim, W. A.: Role of electrostatic interactions in
837 PDZ domain ligand recognition. Biochem., 42, 2797-2805, DOI: 10.1021/bi027061p, 2003.
838 Haugaard-Kedström, L. M., Clemmensen, L. S., Sereikaite, V., Jin, Z., Fernandes, E. F. A., Wind, B.,
839 Abalde-Gil, F., et al.: A High-Affinity Peptide Ligand Targeting Syntenin Inhibits Glioblastoma. J.
840 Med. Chem. 64(3), 1423-1434, DOI: 10.1021/acs.jmedchem.0c00382, 2021.
841 Hegedüs, Z., Hóbor, F., Shoemark, D. K., Celis, S., Lian, L.-Y., Trinh, Ch. H., Sessions, R. B.,
842 Edwards, T. A., Wilson, A. J.: Identification of β-strand mediated protein–protein interaction
843 inhibitors using ligand-directed fragment ligation. Chem. Sci., 12, 2286, DOI: 10.1039/d0sc05694d,
844 2021.
845 Hillier, B. J., Christopherson, K. S., Prehoda, K. E., Bredt, D. S. and Lim, W. A.: Unexpected modes
846 of PDZ domain scaffolding revealed by structure of nNOS–syntrophin complex. Science, 284, 812–
847 815, 1999.
848 Holland, J. D., Klaus, A., Garratt, A. N. and Birchmeier, W.: Wnt signaling in stem and cancer stem
849 cells. Curr. Opin. Cell Biol., 25, 254-264, DOI: 10.1016/j.ceb.2013.01.004, 2013.
850 Hori, K., Ajioky, K., Goda, N., Shindo, A., Tagagishi, M., Tenno, T. and Hiroaki, H.: Discovery of
851 Potent Dishevelled/Dvl Inhibitors Using Virtual Screening Optimized With NMR-Based Docking
852 Performance Index. Front. Pharmacol., 9, 983, DOI: 10.3389/fphar.2018.00983, 2018.
853 Jain, A.K. and Dubes, R.C. Upper Saddle River, NJ: Prentice Hall, Algorithms for clustering data.
854 320p, 1988.
855 Jho, E. H., Zhang, T., Domon, C., Joo, C.-K., Freund, J.-N. and Costantini, F.: Wnt/beta-catenin/Tcf
856 signaling induces the transcription of Axin2, a negative regulator of the signaling pathway. Mol.
857 Cell. Biol., 22, 1172 - 1183, DOI: 10.1128/mcb.22.4.1172-1183.2002, 2002.
858 Kanwar, S. S., Yu, Y., Nautyal, J., Patel, B. B. and Majumdar, A. P. N.: The Wnt/beta-catenin
859 pathway regulates growth and maintenance of colonospheres. Mol. Cancer., 9, 212, DOI:
860 10.1186/1476-4598-9-212, 2010.
861 Kim, H. Y., Choi, S., Yoon, J. H., Lim, H. J., Lee, H., Choi, J., Ro, E. J., Heo, J. N., Lee, W., No, K.
862 T. and Choi, K. Y.: Small molecule inhibitors of the Dishevelled-CXXC5 interaction are new drug
863 candidates for bone anabolic osteoporosis therapy. EMBO Mol. Med., 8, 375-387, DOI:
864 10.15252/emmm.201505714, 2016.
865 Klaus, A. and Birchmeier, W.: Wnt signalling and its impact on development and cancer. Nat. Rev.
866 Cancer, 8, 387-398, DOI: 10.1038/nrc2389, 2008.
867 Kurakin, A., Swistowski, A., Wu, S. C. and Bredesen, D. E.: The PDZ domain as a complex adaptive
868 system. PLoS One, 2(9), e953, DOI: 10.1371/journal.pone.0000953, 2007.
869 Lee, I., Choi, S., Yun, J. H., Seo, S. H., Choi, S., Choi, K. Y. and Lee, W.: Crystal structure of the
870 PDZ domain of mouse Dishevelled 1 and its interaction with CXXC5. Biochem. Biophys. Res.
871 Commun., 485, 584-590, DOI: 10.1016/j.bbrc.2016.12.023, 2017.
872 Lee, H. J., Wang, N. X., Shi, D. L. and Zheng, J. J.: Sulindac inhibits canonical Wnt signaling by
873 blocking the PDZ domain of the protein dishevelled. Angew. Chem. Int. Ed. Engl., 48, 6448 - 6452,
874 DOI: 10.1002/anie.200902981, 2009.
875 Lee, H. J., Wang, X. N., Shao, Y. and Zheng, J.: Identification of tripeptides recognized by the PDZ
876 domain of Dishevelled. Bioorg. Med. Chem., 17, 1701 – 1708, 2009. ,
877 Lewis, A., Segditsas, S., Deheragoda, M., Pollard, P., Jeffery, R., Nye, E., Lockstone, H., Davis, H.,
878 Clark,S., Stamp, G.,Poulsom, R., Wright, N. and Tomlinson, I.: Severe polyposis in Apc(1322T)
879 mice is associated with submaximal Wnt signalling and increased expression of the stem cell marker
880 Lgr5. Gut., 59, 1680 - 1686, DOI: 10.1136/gut.2009.193680, 2010.

881 Lipinski, C. A.: Drug-like properties and the causes of poor solubility and poor permeability. J.
882 Pharmacol. Toxicol. Meth., 44, 235 – 249 . DOI : 10.1016/s1056-8719(00)00107-6, 2000.
883 Lipinski, C. A., Lombardo, F., Dominy, B. W. and Feeney, P. J.: Experimental and computational
884 approaches to estimate solubility and permeability in drug discovery and development settings. Adv.
885 Drug Deliv. Rev., 23, 3 – 25 . DOI : 10.1016/S0169-409X(96)00423-1, 1997.
886 Lv, P. C., Zhu, H. L., Li, H. Q., Sun, J. and Zho, Y.: Synthesis and biological evaluation of pyrazole
887 derivatives containing thiourea skeleton as anticancer. Bioorg. Med. Chem., 18, 4606 - 4614, DOI:
888 10.1016/j.bmc.2010.05.034, 2010.
889 Madrzak, J., Fiedler, M. Johnson, Ch. et al.: Ubiquitination of the Dishevelled DIX domain blocks its
890 head-to-tail polymerization. Nat. Commun., 6, 6718, DOI: 10.1038/ncomms7718, 2015.
891 Malanchi, I., Peinado, H., Kassen, D., Hussenet, T., Metzger, D., Chambon, P., Huber, M., Hohl, D.,
892 Cano, A., Birchmeier, W. and Huelsken, J.: Cutaneous cancer stem cell maintenance is dependent on
893 beta-catenin signalling. Nature., 452, 650 - 653, DOI: 10.1038/nature06835, 2008.
894 Mathvink, R. J., Barritta, A. M., Candelore, M. R., Cascieri, M. A., Deng, L., Tota, L., Strader, C. D.,
895 Wyvratt, M. J., Fosher, M. H. and Weber, A. E.: Potent, elective human beta3 adrenergic receptor
896 agonists containing a substituted indoline-5-sulfonamide pharmacophore. Bioorg. Med. Chem. Lett.,
897 9, 1869 - 1874, DOI: 10.1016/s0960-894x(99)00277-2, 1999.
898 McCoy, A. J., Grosse-Kunstleve, R. W., Adams, P. D., Winn, M. D., Storoni, L. C. and Read, R. J.:
899 Phaser crystallographic software. J. Appl. Cryst., 40(Pt4), 658 - 674, DOI:
900 10.1107/S0021889807021206, 2007.
901 McMartin, C. and Bohacek, R. S.: Powerful, rapid computer algorithms for structure-based drug
902 design, J. Computer-Aided Mol. Des., 11, 333 – 344, DOI: 10.1023/a:1007907728892, 1997.
903 Mizutani, K., Miyamoto, S., Nagahata, T., Konishi, N., Emi, M. and Onda, M.: Upregulation and
904 overexpression of DVL1, the human counterpart of the Drosophila Dishevelled gene, in prostate
905 cancer. Tumori, 91, 546 – 551, 2005.
906 Molenaar, M., van de Wetering, M., Oosterwegegl, M., Peterson-Maduro, J., Godsave, S., Korinek,
907 V., Roose, J., Destrée, O. and Clevers, H.: XTcf-3 transcription factor mediates beta-catenin-induced
908 axis formation in Xenopus embryos. Cell., 86, 391 - 399, DOI: 10.1016/s0092-8674(00)80112-9,
909 1996.
910 Mosmann, T.: Rapid colorimetric assay for cellular growth and survival: application to proliferation
911 and cytotoxicity assays. J. Immunol. Methods., 65, 55 - 63, DOI: 10.1016/0022-1759(83)90303-4,
912 1983.
913 Murshudov, G. N., Vagin, A. A. and Dodson, E. J.: Refinement of macromolecular structures by the
914 maximum-likelihood method. Acta Cryst., 53, 240 - 255, DOI: 10.1107/S0907444996012255, 1997.
915 O'Brien, P. M., Ortwine, D. F., Pavlovsky, A. G., Picard, J. A., Sliskovic, D. R., Roth, B. D., Dyer, R.
916 D., Johnson, L. L., Man, C. F. and Hallak, H.: Structure-activity relationships and pharmacokinetic
917 analysis for a series of potent, systemically available biphenylsulfonamide matrix metalloproteinase
918 inhibitors. J. Med. Chem., 43, 156 - 166, DOI: 10.1021/jm9903141, 2000.
919 Osada, R., Funkhouser, T., Chazelle, D. and Dobkin, D.: Shape distributions, ACM Transactions on
920 Graphics, 21(4), 807 – 832, DOI: 10.1145/571647.571648, 2002
921 Pawson, T.: Dynamic control of signalling by modulator adaptor proteins. Curr. Opin. Cell Biol., 19,
922 112 -116, DOI: 10.1016/j.ceb.2007.02.013, 2007.
923 Polakis, P.: Drugging Wnt signaling in cancer. EMBO J., 31, 2737-2746, DOI:
924 10.1038/emboj.2012.126, 2012.
925 Ponting, C. P., Phillips, C., Davies, K. E. and Blake, D. J.: PDZ domains: targeting signalling
926 molecules to submembranous sites. Bioassays, 19, 469 – 479, DOI: 10.1002/bies.950190606, 1997.
927 Puranik, P., Aakanksha, K., Tadas, S. V., Robert, D. B., Lalji, K. G. and Vincent, C. O. N.: Potent
928 anti-prostate cancer agents derived from a novel androgen receptor down-regulating agent. Bioorg.
929 Med. Chem., 16, 3519 – 3529, DOI: 10.1016/j.bmc.2008.02.031, 2008.
930 Qin, Y., Feng, L., Fan, X., Zheng, L., Zhang, Y., Chang. L., Li, T.: Neuroprotective Effect of N-
931 Cyclohexylethyl-[A/G]-[D/E]-X-V Peptides on Ischemic Stroke by Blocking nNOS–CAPON
932 Interaction. ACS Chem. Neurosci. 12(1), 244-255, DOI: 10.1021/acschemneuro.0c00739, 2021.
933 Riese, J., Yu, X., Munnerly, A., Eresh, L., Hsu, S.-C., Grosschedl, R. and Bienz, M.: LEF-1, a nuclear
934 factor coordinating signaling inputs from wingless and decapentaplegic. Cell, 88, 777 - 787, DOI:
935 10.1016/s0092-8674(00)81924-8, 1997.

936 Rimbault, C., Maruthi, K., Breillat, C., Genuer, C., Crespillo, S., Puente-Muñoz, V., Chamma, I.,
937 Gauthereau, I., Antoine, S., Thibaut, C., Tai, F. W. J., Dartigues, B., Grillo-Bosch, D., Claverol, S.,
938 Poujol, C., Choquet, D., Mackereth, C. D. and Sainlos, M.: Engineering selective competitors for the
939 discrimination of highly conserved protein-protein interaction modules. Nat. Commun., 10, 4521,
940 DOI: 10.1038/s41467-019-12528-4, 2019.
941 Sack, U., Walther, W., Scudiero, D., Selby, M., Aumann, J., Lemos, C., Fichtner, I., Schlag, P. M.,
942 Shoemaker, R. H. and Stein, U.: S100A4-induced cell motility and metastasis is restricted by the
943 Wnt/beta-catenin pathway inhibitor calcimycin in colon cancer cells. Mol. Biol. Cell., 22, 3344 -
944 3354, DOI: 10.1091/mbc.E10-09-0739, 2011.
945 Sanner, M. F, Olson, A. J. and Spehner, J. C.: Reduced surface: an efficient way to compute molecular
946 surfaces, Biopolymers, 38, 305 – 320, DOI: 10.1002/(SICI)1097-0282(199603)38:3%3C305::AID-
947 BIP4%3E3.0.CO;2-Y, 1996.
948 Saupe, J., Roske, Y., Schillinger, C., Kamdem, N., Radetzki, S., Diehl, A., Oschkinat, H., Krause, G.,
949 Heinemann, U. and Rademann, J.: Discovery, structure-activity relationship studies, and crystal
950 structure of non-peptide inhibitors bound to the Shank3 PDZ domain. ChemMedChem, 6, 1411 -
951 1422, DOI: 10.1002/cmdc.201100094, 2011.
952 Schultz, J., Hoffmüller, U., Krause, G., Ashurts, J., Macias, M. J., Schmieder, P., Schneider-Mergener,
953 J. and Oschkinat, H.: Specific interactions between the syntrophin PDZ domain and voltage-gated
954 sodium channels. Nat. Struct. Biol., 5, 19 – 24, DOI: 10.1038/nsb0198-19, 1998.
955 Schwarz-Romond, T., Fiedler, M., Shibata, N., Butler, P.J.G., Kikuchi, A., Higuchi, Y., Bienz, M.:
956 The DIX domain of Dishevelled confers Wnt signaling by dynamic polymerization. Nat. Struct. Mol.
957 Biol., 14(6), 484-492, DOI: 10.1038/nsmb1247, 2007.
958 Shan, J., Shi, D. L., Wang, J. and Zheng, J.: Identification of a specific inhibitor of the dishevelled
959 PDZ domain. Biochem., 44, 15495-15503, DOI: 10.1021/bi0512602, 2005.
960 Shan, J., Zhang, X., Bao, J., Cassell, R. and Zheng, J. J.: Synthesis of potent Dishevelled PDZ domain
961 inhibitors guided by virtual screening and NMR studies, Chem. Biol. Drug. Des., 79, 376 – 383,
962 DOI: 10.1111/j.1747-0285.2011.01295.x, 2012.
963 Sheng, M. and Sala, C.: PDZ domains and the organization of supramolecular complexes. Annu. Rev.
964 Neurosci., 24, 1 – 29, DOI: 10.1146/annurev.neuro.24.1.1, 2001.
965 Sievers, F., Wilm, A., Dineen, D. G., Gibson, T. J., Karplus, K., Li, W., Lopez, R., McWilliam, H.,
966 Remmert, M., Söding, J., Thompson, J. D. and Higgins, D. G.: Fast, Scalable generation of high-
967 quality protein multiple sequence alignments using Clustal Omega. Mol. Syst. Biol., 7, 539,
968 Doi:10.1038/msb.2011.75, 2011.
969 Sineva, G. S. and Pospelov, V. A.: Inhibition of GSK3beta enhances both adhesive and signalling
970 activities of beta-catenin in mouse embryonic stem cells. Biol. Cell, 102, 549-560, DOI:
971 10.1042/BC20100016, 2010.
972 Sleight, A. J., Boess, F. G., Bös, M., Levet-Trafit, B., Riemer, C. and Bourson, A. Br.:
973 Characterization of Ro 04-6790 and Ro 63-0563: potent and selective antagonists at human and rat
974 5-HT6 receptors. J. Pharmacol., 124, 556 - 562, DOI: 10.1038/sj.bjp.0701851, 1998.
975 Songyang, Z., Fanning, A. S., Fu, C., Xu, J., Marfatia, S. M., Chisti, A. H., Crompton, A., Chan, A.
976 C., Anderson, J. M. and Cantley, L. C.: Recognition of unique carboxyl-terminals motifs by distinct
977 PDZ domains. Science, 275, 73 - 77, DOI: 10.1126/science.275.5296.73, 1997.
978 Shuker, S. B., Hajduk, P. J., Meadows, R. P. and Fesik, S. W.: Discovering high-affinity ligands for
979 proteins: SAR by NMR. Science, 274, 1531 – 1534, DOI: 10.1126/science.274.5292.1531, 1996.
980 Tellew, J. E., Baska, R. A. F., Beyer, S. M., Carlson, K. E., Cornelius, L. A., Fadnis, L., Gu, Z., Kunst,
981 B. L., Kowala, M. C., Monshizadegan, H., Murugesan, N., Ryan, C. S., Valentine, M. T., Yang, Y.
982 and Macor, J. E.: Discovery of 4-[(imidazol-1-yl)methyl]biphenyl-2-sulfonamides as dual
983 endothelin/angiotensin II receptor antagonists. Bioorg. Med. Chem. Letters,13, 1093 – 1096, DOI:
984 10.1016/s0960-894x(03)00018-0, 2003.
985 The PyMOL Molecular Graphics System, Version 2.3.4 Schrödinger, LLC
986 Uematsu, K., He, B., You, L., Xu, Z., McCormick, F. and Jablons, D. M.: Activation of the Wnt
987 pathway in non-small cell lung cancer: evidence of dishevelled overexpression. Oncogene, 22, 7218
988 - 7221, DOI: 10.1038/sj.onc.1206817, 2003.
989 Uematsu, K., Kanazawa, S., You, L., He, B., Xu, Z., Li, K., Peterlin, B. M., McCormick, F. and
990 Jablons, D. M.: Wnt pathway activation inmesothelioma: evidence of dishevelled overexpression and
991 transcriptional activity of β-catenin. Cancer Res., 63, 4547 – 4551, 2003.

992 Vermeulen, L., De Sousa E Melo, F., van der Heijden, M., Cameron, K., de Jong, J. H., Borovski, T.,
993 Tuynman, J. B., Todaro, M., Merz, C., Rodermond, H., Sprick, M. R., Kemper, K., Richel, J. J.,
994 Stassi, G. and Medema, J. P.: Wnt activity defines colon cancer stem cells and is regulated by the
995 microenvironment. Nat. Cell. Biol., 12, 468 - 476, DOI: 10.1038/ncb2048, 2010.
996 Wallingford, B. J. and Raymond H.: The developmental biology of Dishevelled: an enigmatic protein
997 governing cell fate and cell polarity. Development, 132, 4421 - 4436, DOI: 10.1242/dev.02068,
998 2005.
999 Wang, C., Dai, J., Sun, Z., Shi, C., Cao, H., Chen, X., Gu, S., Li, Z., Qian, W. and Han, X.: Targeted
1000 inhibition of dishevelled PDZ domain via NSC668036 depresses fibrotic process. Exp. Cell Res.,
1001 331, 115 – 122, DOI: 10.1016/j.yexcr.2014.10.023, 2015.
1002 Weeraratna, A. T., Jiang, Y., Hostetter, G., Rosenblatt, K., Duray, P., Bittner, M. and Trent. J. M.:
1003 Wnt5a signalling directly affects cell motility and invasion of metastic melanoma. Cancer Cell, 1,
1004 279 – 288, DOI: 10.1016/s1535-6108(02)00045-4, 2002.
1005 Wong, H. C., Bourdelas, A., Krauss, A., Lee, H. J., Shao, Y., Wu, D., Mlodzik, M., Shi, D. L. and
1006 Zheng, J.: Direct binding of the PDZ domain of Dishevelled to a conserved internal sequence in the
1007 C-terminal region of Frizzled J. Mol. Cell, 12, 1251 -1260, DOI: 10.1016/s1097-2765(03)00427-1,
1008 2003.
1009 Wong, H., Mao, J., Nguyen, J. T., Srinivas, S., Zhang, W., Liu, B., Li, L., Wu, D. and Zheng, J.:
1010 Structural basis of the recognition of the dishevelled DEP domain in the Wnt signalling pathway.
1011 Nat. Struct. Biol., 7, 1178 -1184, DOI: 10.1038/82047, 2000.
1012 Wu, C., Decker, E. R., Blok, N., Bui, H., Chen, Q., Raju, B., Bourgoyne, A. R., Knowles, V.,
1013 Biediger, R. J., Market, R. V., Lin, S., Dupre, B., Kogan, T. P., Holland, G. W., Brock, T. A. and
1014 Dixon, R. A. F.: Endothelin antagonists: substituted mesitylcarboxamides with high potency and
1015 selectivity for ET(A) receptors. J. Med. Chem., 42, 4485 - 4499, DOI: 10.1021/jm9900063, 1999.
1016 Zartler, E. R. and Shapiro, M. J.: Protein NMR-based screening in drug discovery. Curr. Pharm. Des.,
1017 12, 3963 – 3972, DOI: 10.2174/138161206778743619, 2006.
1018 Zartler, E. R., Hanson, J., Jones, B. E., Kline, A. D., Martin, G., Mo, H., Shapiro, M. J., Wang, R.,
1019 Wu, H. and Yan, J.: RAMPED-UP NMR: multiplexed NMR-based screening for drug discovery. J.
1020 Am. Chem. Soc., 125, 10941 - 10946, DOI: 10.1021/ja0348593, 2003.
1021 Zhang, M. and Wang, W.: Organization of signalling complexes by PDZ-domain scaffold proteins.
1022 Acc. Chem. Res., 36, 530 – 538, DOI: 10.1021/ar020210b, 2003.
1023 Zhang, Y., Appleton, B. A., Wiesmann, C., Lau, T., Costa, M., Hannoush, R. N. and Sidhu, S. S.:
1024 Inhibition of Wnt signaling by Dishevelled PDZ peptides. Nat. Chem. Biol., 5, 217 -219, DOI:
1025 10.1038/nchembio.152, 2009.